nature structural & molecular biology

Article

https://doi.org/10.1038/s41594-024-01395-3

Catalytic and noncatalytic functions of DNA polymerase κ in translesion DNA synthesis

Received: 1 September 2023

Accepted: 28 August 2024

Published online: 19 September 2024

Check for updates

Selene Sellés-Baiget[1], Sara M. Ambjørn[1,8], Alberto Carli[2,8], Ivo A. Hendriks[1,8], Irene Gallina[1,3], Norman E. Davey[4], Bente Benedict[1,5], Alessandra Zarantonello[1,5], Sampath A. Gadi[1,5], Bob Meeusen[1], Emil P. T. Hertz[1], Laura Slappendel[6], Daniel Semlow[7], Shana Sturla[6], Michael L. Nielsen[1], Jakob Nilsson[1], Thomas C. R. Miller[2] & Julien P. Duxin[1,5]

Translesion DNA synthesis (TLS) is a cellular process that enables the bypass of DNA lesions encountered during DNA replication and is emerging as a primary target of chemotherapy. Among vertebrate DNA polymerases, polymerase κ (Polκ) has the distinctive ability to bypass minor groove DNA adducts in vitro. However, Polκ is also required for cells to overcome major groove DNA adducts but the basis of this requirement is unclear. Here, we combine CRISPR base-editor screening technology in human cells with TLS analysis of defined DNA lesions in *Xenopus* egg extracts to unravel the functions and regulations of Polκ during lesion bypass. Strikingly, we show that Polκ has two main functions during TLS, which are differentially regulated by Rev1 binding. On the one hand, Polκ is essential to replicate across a minor groove DNA lesion in a process that depends on PCNA ubiquitylation but is independent of Rev1. On the other hand, through its cooperative interaction with Rev1 and ubiquitylated PCNA, Polκ appears to stabilize the Rev1–Polζ extension complex on DNA to allow extension past major groove DNA lesions and abasic sites, in a process that is independent of Polκ's catalytic activity. Together, our work identifies catalytic and noncatalytic functions of Polκ in TLS and reveals important regulatory mechanisms underlying the unique domain architecture present at the C-terminal end of Y-family TLS polymerases.

Lesions generated in DNA can impede DNA synthesis. High-fidelity replicative polymerases are unable to accommodate DNA lesions in their catalytic site because of the resultant distortion in DNA geometry[1,2]. This often leads to replication fork uncoupling, activation of the replication checkpoint and replication stress[3].

DNA lesions encountered during replication can be bypassed by DNA damage tolerance (DDT) mechanisms[4]. Two distinct DDT mechanisms have been described: template switching (TS), which relies on a recombination-based process to copy genetic information from the undamaged sister chromatid, and translesion DNA synthesis (TLS), which involves specialized DNA polymerases to synthesize across damaged bases[5]. Unlike replicative polymerases, TLS polymerases exhibit poor processivity and low fidelity. This is attributed to the lack of proofreading activity and the presence of a flexible catalytic site that can accommodate damaged DNA bases[1,2]. Ubiquitylation of proliferating cell nuclear antigen (PCNA) on K164 stimulates both TLS and TS processes[6–8]. This is because most enzymes participating in DDT contain PCNA-binding and ubiquitin-binding motifs that bind to ubiquitylated PCNA and are thereby targeted to lesion sites[9].

A full list of affiliations appears at the end of the paper. e-mail: Julien.duxin@bric.ku.dk

In vertebrates, the TLS polymerases operating during replication are polymerase η (Polη), Polι, Polκ and Rev1, which are classified under the Y-family, and Polζ, which is a member of the B-family. Although a single polymerase may catalyze both steps of DNA lesion bypass (incorporation of a nucleotide opposite the DNA lesion and the subsequent extension past the lesion), TLS often involves the actions of an 'inserter' and an 'extender' (ref. 9). An example of an insertion polymerase is Polη, which effectively bypasses ultraviolet (UV)-induced thymine–thymine cyclobutane pyrimidine dimers (CPDs)[10–12]. In contrast, Polζ is a multisubunit TLS polymerase known for its ability to extend mismatched DNA termini, which can originate from nucleotides inserted by Y-family polymerases[13,14]. This process is observed during the bypass of UV-induced 6–4 photoproducts, cisplatin-induced intrastrand crosslinks, and M.HpaII DNA–protein crosslinks (DPCs). In each of these scenarios, Polζ extends the mispaired nucleotide(s) inserted by Polη[15–18].

Despite its deoxycytidyl transferase activity, Rev1 is best known for its scaffolding role on Polζ and other Y-family polymerases[19,20]. In fact, Rev1 is an integral component of Polζ in yeast and in *Xenopus* egg extracts[21,22]. Rev1 also stimulates the recruitment of Y-family polymerases to lesion sites. This process can occur independently of PCNA ubiquitylation and offers TLS polymerases an alternative recruitment platform[19,23]. Consistent with this, Y-family polymerases contain C-terminal regions composed of multiple protein–protein interaction domains that mediate binding to PCNA, ubiquitin and Rev1. However, the interplay between Rev1 and ubiquitylated PCNA in targeting TLS polymerases to lesion sites remains unclear.

In contrast to Polη, Rev1 and Polζ, the role of Polκ in TLS remains poorly defined. Polκ shares homology with bacterial DinB[24,25]. In vitro, both DinB and Polκ can bypass adducts located in the minor groove of DNA, which do not fit in the active site of other TLS polymerases[26,27]. This is because Polκ contains a unique N-clasp and polymerase-associated domain (PAD) that allow its catalytic core to open toward the minor groove of DNA[28,29]. Minor groove adducts include N^2-adducted guanosines generated by alkylating agents such as benzo[a]pyrene and acylfuvenes[26,30,31]. Similarly, illudin S and mitomycin C (MMC) generate minor groove DNA lesions, albeit with different chemistries[32,33]. Consistent with this, Polκ-deficient cells are exquisitely sensitive to both illudin S and MMC[34–36]. However, formal proof that Polκ enables the bypass of minor groove DNA lesions during replication is still lacking.

Intriguingly, Polκ-deficient cells are also sensitive to major groove DNA-damaging agents, such as UV radiation and cisplatin[35–38], despite Polκ being unable to synthesize across UV lesions in vitro[39]. This suggests that Polκ may function in TLS independently of its catalytic activity. This was proposed on the basis of the sensitivity to different DNA-damaging agents of cells expressing a catalytic-deficient Polκ[40] but the mechanism underlying this function is unknown. In addition, Polκ has also been involved in nucleotide excision repair (NER) in both mammalian cells and *Xenopus* egg extracts[36,37,41]. Polκ was also suggested to participate in the restart of stalled replication forks and the activation of the replication checkpoint[42–44].

How Polκ is recruited to DNA lesions remains unclear. Like all Y-family polymerases, Polκ contains a long and flexible C-terminal end that mediates interactions with ubiquitylated PCNA[45]. In fact, Polκ contains two PCNA-interacting protein (PIP) motifs and two ubiquitin-binding zinc finger (UBZ) domains that may differently contribute to Polκ targeting to lesion sites[46]. Moreover, if Polκ can be targeted by PCNA ubiquitylation, why does it also contain a conserved Rev1-interacting region (RIR)? In this regard, the Polκ–Rev1 interaction was shown to mediate the formation of a stable Polκ–Rev1–Polζ complex in vitro[47] but the relevance of this complex is also unknown. In summary, while Polκ catalytic function has been studied in vitro, the roles and regulations of Polκ during DNA replication remain elusive, particularly with regard to its function across major groove DNA lesions.

Here, we elucidate the roles and regulations of Polκ during DNA replication across defined DNA lesions. By combining clustered regularly interspaced short palindromic repeats (CRISPR) base-editor screening technology in human cells with TLS analysis of defined DNA lesions in *Xenopus* egg extracts, we demonstrate that TLS across a minor groove DNA lesion requires Polκ's catalytic activity. While this function depends on Polκ's interaction with ubiquitin and PCNA, it is independent of Rev1. In contrast, we find that a Polκ–Rev1 interaction is essential to stimulate the bypass of major groove DNA lesions and abasic (AP) sites that require Polζ-mediated extension. Using its flexible C-terminal end, which can cooperatively bind to Rev1 and ubiquitylated PCNA, Polκ appears to stabilize the Rev1–Polζ complex on damaged chromatin, allowing extension past DNA lesions in a process that is independent of Polκ's catalytic activity. Collectively, our results unravel the multifaceted functions and regulations of Polκ during TLS.

Results

Polκ is required to bypass minor groove adducts

Polκ-deficient cells are exquisitely sensitive to agents that damage the minor groove of DNA such as illudin S[35]. To understand the role of Polκ's functional domains in counteracting illudin S-mediated damage, we first performed a CRISPR–Cas9 base-editor tiling screen in the presence and absence of illudin S. We designed a single guide RNA (sgRNA) lentiviral library aimed at introducing missense mutations along the Polκ coding sequence. The sgRNA library was cloned into

Fig. 1 | Polκ is essential to bypass minor groove DNA lesions. a, Schematic outline of a Polκ CRISPR base-editor tiling screen aimed at identifying missense mutations that sensitize RPE1-hTERT *p53*$^{-/-}$ cells to illudin S. NGS, next-generation sequencing. **b**, Dot plot showing the results of the Polκ CRISPR base-editor tiling screen. Each guide is shown as a dot. The *x* axis represents the amino acid position in Polκ that is targeted for point substitution. The *y* axis represents the $\log_2$(fold change) between illudin S and untreated conditions. Larger dots represent guides that significantly change in illudin S (*P* value ≤ 0.01). The various domains of Polκ are indicated. **c**, Composite molecular model of human Polκ with the predicted point substitutions (in red) derived from the base-editor tiling screen that sensitized cells to illudin S treatment. Dashed lines represent disordered regions that are not present in the model. The model was generated by combining structure predictions from AlphaPulldown[77] and AlphaFold2 (ref. 78), as described in the Methods, along with deposited structures of human Polκ and PCNA (PDB 5W2C (ref. 79), PDB 6TNY (ref. 55) and PDB 3TBL (ref. 80)). **d**, Left, schematic of p3d-Phen-A. Right, scheme displaying the leftward nascent leading strand and extension products during replication of p3d-Phen-A generated upon HaeII and HindIII digest. Double digestion generates longer damaged and shorter undamaged extension products, which can be resolved on a denaturing polyacrylamide gel. The leftward CMG helicase is depicted in green, while the minor groove adduct is depicted in blue. **e**, p3d-Phen-A was replicated in the presence or absence of a ubiquitin E1 inhibitor (MLN-7243). Reaction samples were digested with HaeII and HindIII followed by separation on a denaturing polyacrylamide gel alongside a sequencing ladder. The stalling points position in relationship to the minor groove adduct are shown in the lower radiograph. The upper radiograph shows the extension products; note that ~70% of the plasmid preparation contains the adduct. **f**, Polκ-depleted extracts were compared to a mock depletion dilution series. Polκ-depleted extracts were supplemented with buffer, WT Polκ or CD Polκ. Samples were blotted with the indicated antibodies. The asterisk denotes a nonspecific band. **g**, Schematic diagram illustrating the replication intermediates generated during the replication of p3d-Phen-A. **h**, Samples from **f** were used to replicate p3d-Phen-A in the presence of [α-^{32}P]dATP. Reaction samples were analyzed by native agarose gel electrophoresis. RI, replication intermediate. Red arrowheads indicate the accumulation of OC molecules. Note that accumulated OC molecules undergo 5′-to-3′ resection over time, leading to faster migration on the gel. **i**, Samples from **h** were digested with HaeII and HindIII analyzed as in **e**.

https://doi.org/10.1038/s41594-024-01395-3

ABE8e-SpG[48], which introduces A→G conversions in defined proximity to the sgRNA-binding site. Using this library, we targeted >50% of Polκ amino acids with point substitutions (Supplementary Table 1). Briefly, RPE1-hTERT *p53*$^{-/-}$ cells were transduced with the lentiviral sgRNA library. After selection, cells were cultured in the presence or absence of a low dose of illudin S for 12 additional days. Subsequently, sgRNAs were quantified by next-generation sequencing to identify edits that conferred sensitivity to illudin S (Fig. 1a and Supplementary

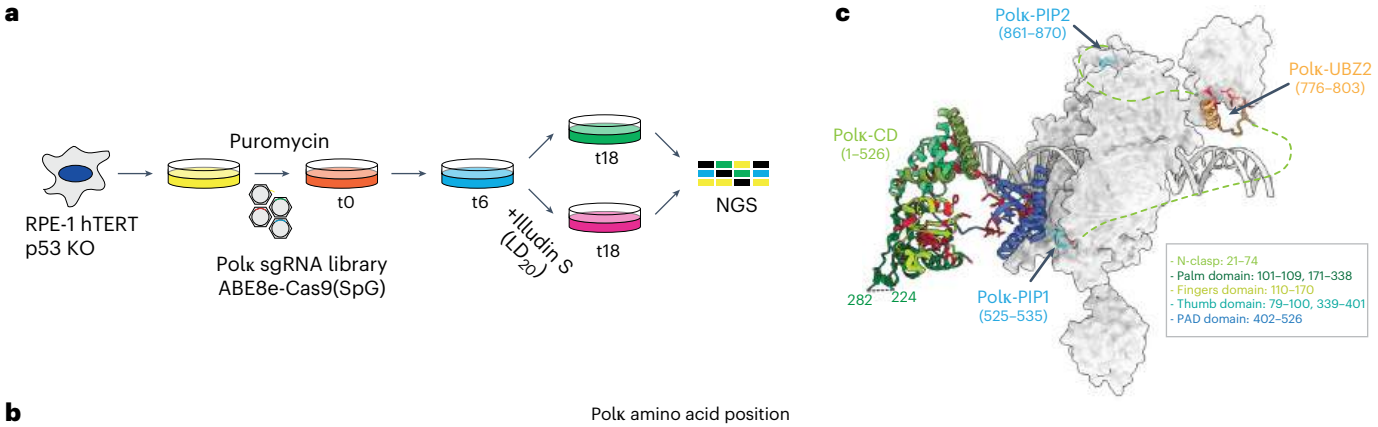

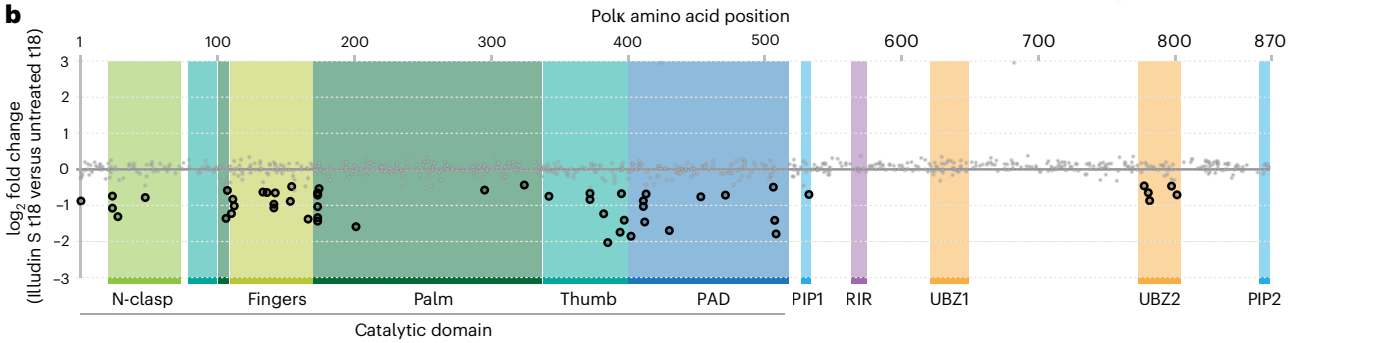

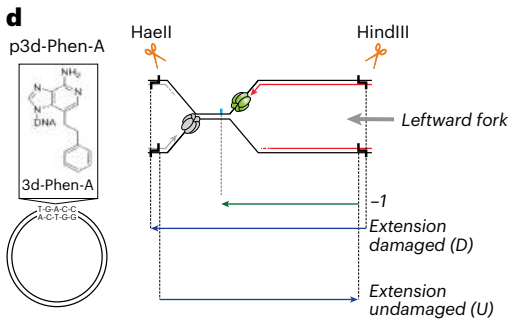

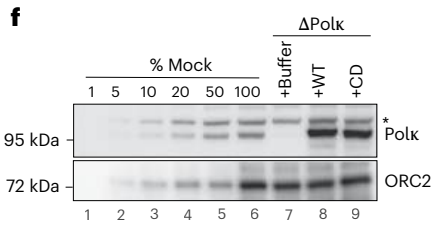

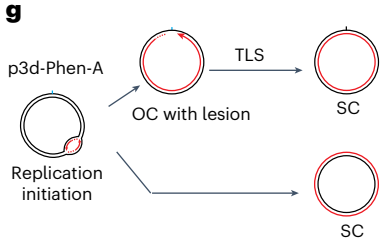

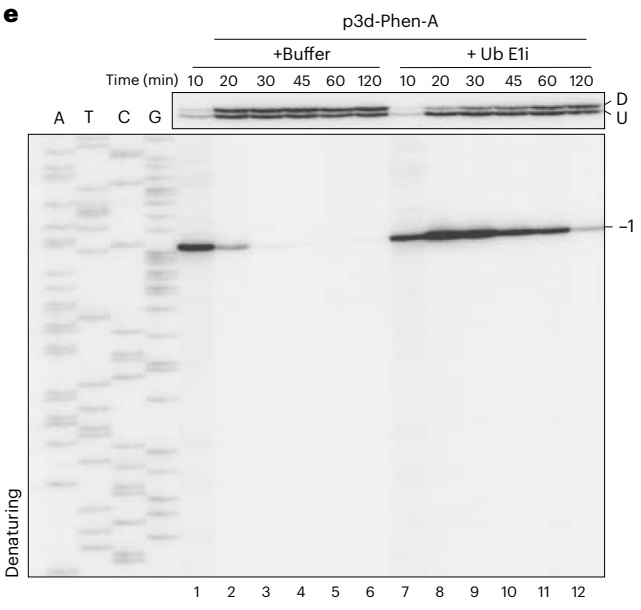

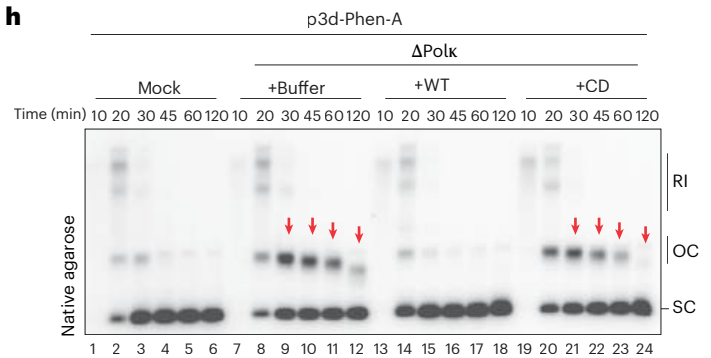

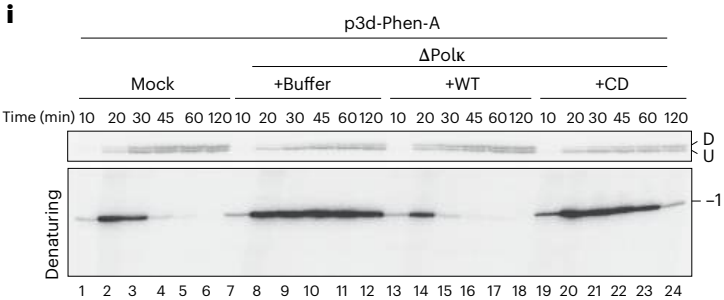

Table 1). Consistent with Polκ's unique ability to bypass minor groove DNA adducts in vitro, numerous sgRNAs predicted to cause point substitutions in the catalytic domain of Polκ severely sensitized cells to illudin S without affecting the untreated condition (Fig. 1b and Extended Data Fig. 1a). These included sgRNAs targeting the N-clasp, PAD and palm and finger domains, which are essential for Polκ's TLS properties (Fig. 1b,c and Extended Data Fig. 1b,c)[28,29,49]. Outside of the catalytic domain, sgRNAs targeting Polκ's PIP1 (known to bind PCNA) and UBZ2 (known to bind ubiquitin) were the only sgRNAs that also sensitized cells to illudin S (Fig. 1b,c and Extended Data Fig. 1b,c). In contrast, Polκ's RIR, UBZ1 and PIP2 did not score, despite the screen containing several sgRNAs targeting these regions. This suggests that these domains may be dispensable to confer illudin S resistance, although we cannot exclude a low editing efficiency resulting in a lack of effect. Taken together, these results suggest that Polκ is targeted to minor groove DNA lesions by binding to ubiquitylated PCNA (through its PIP1 and UBZ2) in a process that may be independent of Rev1.

To validate our screen and monitor replication across minor groove DNA lesions, we used the *Xenopus* egg extract system, which recapitulates DNA replication and TLS[15,50]. To this end, we generated a plasmid containing a site-specific 3-deaza-3-phenethyl-adenosine acylfulvene minor groove DNA adduct (p3d-Phen-A) (Fig. 1d, left)[31] and replicated it in egg extracts supplemented with [α-^{32}P]-labeled deoxyadenosine triphosphate ([α-^{32}P]dATP). We then tested whether the bypass of this lesion requires TLS by comparing p3d-Phen-A replication with a control plasmid (pCTRL) in the presence or absence of a ubiquitin E1 inhibitor[15]. While the E1 inhibitor did not affect pCTRL replication (Extended Data Fig. 1d, lanes 1–12), it stabilized open circular (OC) molecules during p3d-Phen-A replication (lanes 13–24). This stabilization suggests a TLS defect in the absence of de novo ubiquitylation, leading to the accumulation of OC molecules originating from the adducted parental strand (Extended Data Fig. 1e).

To understand how the minor groove adduct is bypassed, we analyzed replication intermediates on a denaturing gel following digest with HaeII and HindIII (Fig. 1d, right). During the replication of p3d-Phen-A, we observed a specific −1 product (Fig. 1e, lanes 1 and 2). This product disappeared after 20–30 min, correlating with the appearance of extended products (Fig. 1e, lanes 2–6). This is consistent with nascent-strand synthesis first stalling at the adduct and then bypassing the lesion through TLS. In contrast, in the presence of the ubiquitin E1 inhibitor, nascent-strand synthesis also stalled at −1 but persisted up to 2 h, suggesting severe TLS inhibition (Fig. 1e, lanes 7–12).

Next, we investigated whether Polκ is required for bypass of the minor groove adduct. To this end, we depleted Polκ from extracts and replicated p3d-Phen-A (Fig. 1f and Extended Data Fig. 1f). In the absence of Polκ, conversion of OC to supercoiled (SC) molecules was impaired (Figs. 1g,h, lanes 7–12, red arrows) and nascent strands persisted at −1 (Fig. 1i, lanes 7–12), indicating the absence of TLS. Polκ-depleted extracts were also supplemented with recombinant Polκ wild type (WT) or a catalytically inactive mutant harboring D199A and E200A substitutions (CD) (Fig. 1f and Extended Data Fig. 1g)[24], which is deficient in DNA synthesis (Extended Data Fig. 1h). TLS was restored by the addition of Polκ WT but not Polκ CD (Fig. 1h,i, lanes 13–24), confirming that the catalytic activity of Polκ is required to bypass the minor groove DNA lesion. Thus, *Xenopus* egg extracts are an ideal system to study the functions and regulations of Polκ during TLS.

Polκ bypass of a minor groove lesion is independent of Rev1

We next examined the functional domains of Polκ that are required for bypassing the minor groove adduct. To this end, we generated different point mutants of Polκ deficient in PCNA, Rev1 or ubiquitin binding (Fig. 2a)[45,51–53], which we added back to Polκ-depleted extracts. Consistent with our tiling screen, the Polκ depletion effect was rescued by the addition of Polκ RIR* (Fig. 2b, lanes 13–16, and Extended Data Fig. 2a,b). Moreover, depletion of Rev1 had no impact on the replication of p3d-Phen-A, which was exclusively dependent on Polκ (Fig. 2c). Thus, Polκ's catalytic activity across the minor groove DNA lesion is independent of Rev1.

Analysis of Polκ's PCNA-interacting motifs revealed that both PIP1 and PIP2 contribute to Polκ-mediated bypass. As seen in Fig. 2d (lanes 13–16 and 17–20), addition of Polκ PIP1 or PIP2 mutant partially restored TLS but not as efficiently as the WT protein (Extended Data Fig. 2c,d). Moreover, addition of a double PIP mutant further impaired Polκ's function, leading to nascent strands persisting at −1 for 120 min (Fig. 2d, lanes 21–24, and Extended Data Fig. 2d). We conclude that both PIPs can contribute to Polκ's TLS activity across the minor groove adduct. However, in line with previous work showing that PIP1 but not PIP2 is required for Polκ-mediated synthesis[54,55] and our base-editor screen where PIP1 but not PIP2 targeting sensitized cells to illudin S, we envision that Polκ's PIP1 is the primary PCNA interactor during catalysis. We hypothesize that PIP2 may act as a recruitment or structural stabilizer by binding to a second PCNA molecule (Discussion).

Lastly, analysis of Polκ's UBZs further agreed with our screen and revealed that UBZ2 but not UBZ1 is important for Polκ's function (Fig. 2e and Extended Data Fig. 2e,f). We conclude that Polκ's catalytic activity across a minor groove lesion is independent of Rev1 and may solely depend on PCNA ubiquitylation (Discussion).

Polκ's RIR is required to bypass a major grove DPC

Rev1 is a scaffolding protein that facilitates the recruitment of Y-family TLS polymerases to damaged DNA through their RIR domain[9]. Surprisingly, we found that Polκ's RIR is dispensable for bypassing a minor groove adduct, prompting the question of when the Polκ–Rev1 interaction becomes necessary.

We previously showed that both Polκ and Rev1 are synchronously enriched on DNA during replication of a major groove M.HpaII DPC-containing plasmid[56]. When this lesion is encountered by the replisome, the DPC is first degraded by the SPRTN protease and/or the proteasome, leading to the formation of a peptide–DNA adduct that is then bypassed by TLS (Extended Data Fig. 3a)[56,57]. TLS across a M.HpaII peptide adduct is a two-step mutagenic process, in which Polη inserts one or two nucleotides across the damaged base, followed by Polζ-mediated extension past the lesion[15,57]. In the absence of Polη, Polζ performs both insertion and extension, but with higher mutagenesis[15]. The recruitment of Polκ to the DPC plasmid (Fig. 3a)[56] raised the possibility that Polκ may also have a function in the bypass of this major groove lesion.

To test this, we first replicated the M.HpaII DPC plasmid (pDPC) in mock or Polκ-depleted extracts. As a control, pDPC was also replicated in Polη-depleted or Rev1-depleted extracts (Extended Data Fig. 3b; note that Rev1 codepletes Polζ)[15,22]. As previously shown, while depletion of Polη had little impact on the conversion of OC to SC molecules (Extended Data Fig. 3c, lanes 6–10), depletion of Rev1 stabilized OC molecules for up to 240 min, consistent with no bypass of the peptide–DNA adduct (Extended Data Fig. 3c, lanes 16–20, red arrows)[15,57]. Strikingly, in the absence of Polκ, conversion of OC to SC molecules was also impaired, suggesting the absence of TLS (Extended Data Fig. 3c, lanes 11–15, red arrows). To understand how Polκ depletion affects replication across the DPC, nascent leading strands were analyzed on a denaturing gel (Fig. 3b). During replication of pDPC, nascent-strand synthesis first stalls ~30–40 nt upstream of the DPC (Fig. 3c, lane 1). Following CMG bypass of the DPC, the nascent strand advances to the lesion site where it stalls at the −1, 0 and +1 positions (Fig. 3c, lanes 2 and 3). The nascent strand is then extended past the lesion and extension products appear by 120 min (Fig. 3c, lanes 3–5, top radiograph). While insertion across the lesion was dependent on Polη (Fig. 3c, lanes 6–10), extension past the lesion required Rev1–Polζ (Fig. 3c, lanes 16–20), as previously described[15]. Surprisingly, in the absence of Polκ, nascent strands reached the crosslink with normal kinetics but also permanently stalled at −1, 0 and +1, mimicking Rev1–Polζ depletion

https://doi.org/10.1038/s41594-024-01395-3

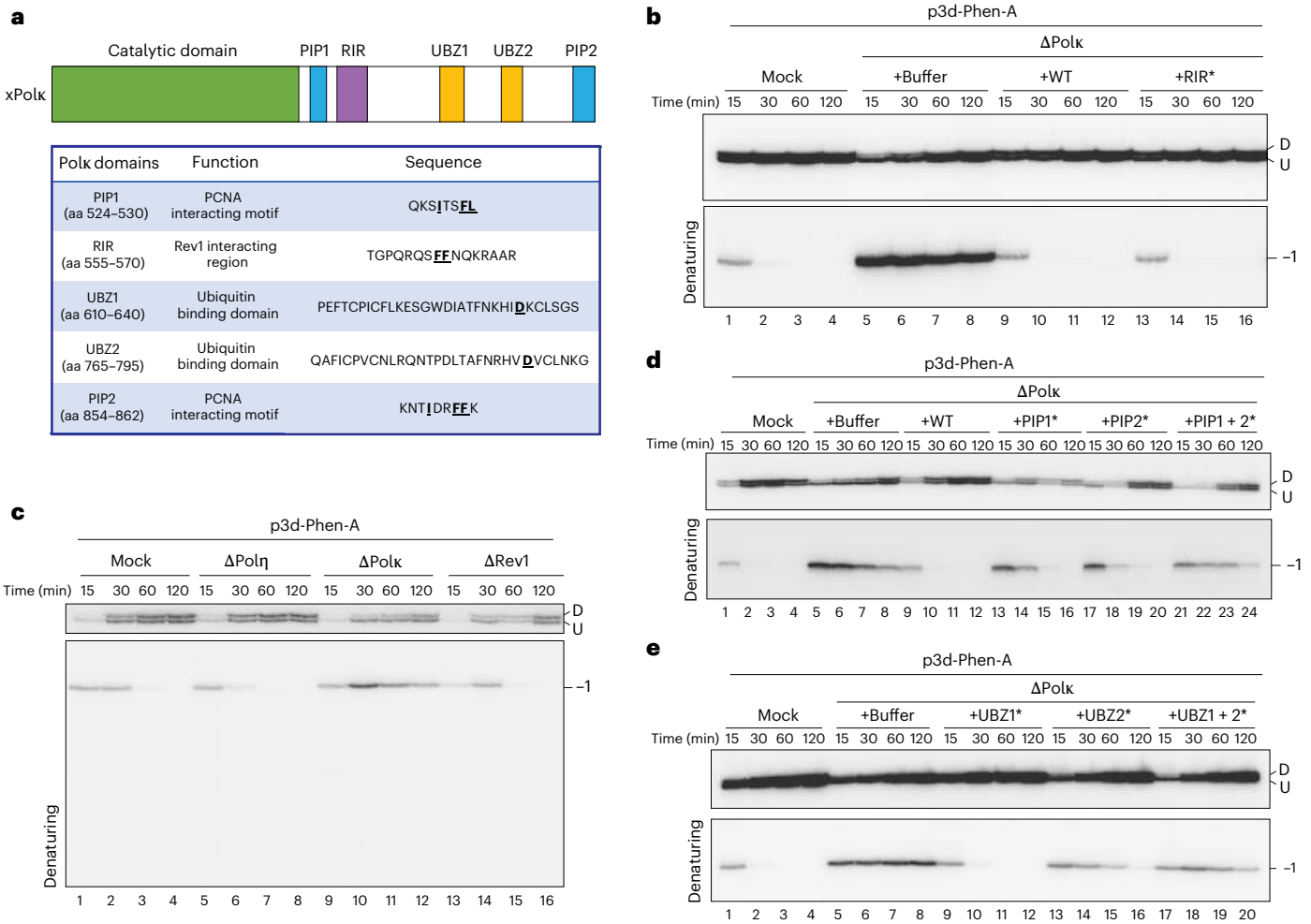

Fig. 2 | Polκ-mediated bypass of minor groove lesions is independent of Rev1. **a**, Overview of *Xenopus* Polκ and the specific point mutants used in this study. The underlined amino acids within each domain sequence were substituted to alanine. **b**, Mock and Polκ-depleted egg extracts were used to replicate p3d-Phen-A. Polκ-depleted extracts were supplemented with buffer, recombinant WT Polκ or RIR* mutant Polκ. Samples were digested and analyzed as in Fig. 1e. **c**, p3d-Phen-A was replicated in mock, Polη-depleted, Polκ-depleted or Rev1-depleted extracts. Samples were digested and analyzed as in Fig. 1e. **d**, Mock and Polκ-depleted egg extracts were supplemented with buffer, recombinant WT Polκ or PIP1, PIP2 or PIP1 and PIP2 mutant Polκ. Extracts were then used to replicate p3d-Phen-A. Samples were digested and analyzed as in Fig. 1e. **e**, Mock and Polκ-depleted egg extracts were supplemented with buffer or UBZ1, UBZ2 or UBZ1 and UBZ2 mutant Polκ. Extracts were then used to replicate p3d-Phen-A. Samples were digested and analyzed as in Fig. 1e.

(Fig. 3c, lanes 11–15). This was not because of codepletion of Rev1–Polζ with the anti-Polκ antibody (Extended Data Fig. 3b). Similarly, Polκ was not codepleted upon Rev1–Polζ depletion (Extended Data Fig. 3b). Collectively, these results indicate that Polκ has an essential role in TLS extension past M.HpaII DPC lesions.

Next, we investigated whether the Polκ–Rev1 interaction is needed for this process. To this end, we performed rescue experiments with WT and RIR mutant Polκ. While the addition of WT Polκ restored TLS, addition of RIR mutant Polκ failed to do so (Fig. 3d,e). Thus, in contrast to Polκ-mediated TLS of the minor groove adduct, the Polκ–Rev1 interaction through Polκ's RIR is needed for the bypass of a major groove DPC.

Polκ's noncatalytic function during DPC bypass

Next, we investigated whether Polκ activity stimulates extension past the peptide–DNA adduct and performed rescue experiments with WT or CD Polκ. Strikingly, addition of WT or CD Polκ rescued the extension defect caused by Polκ depletion (Fig. 4a,b), indicating that Polκ has a noncatalytic function in stimulating TLS across the DPC. Consistent with this, when Rev3, the catalytic subunit of Polζ, was depleted from extracts (Extended Data Fig. 3b), extension was also abolished (Extended Data Fig. 3d), confirming that Polζ provides the extension activity across the DPC substrate. Identical results were obtained if pDPC was pretreated with proteinase K to digest the DPC into a short peptide adduct[57], indicating that the role of Polκ in pDPC replication is independent of DPC proteolysis (Extended Data Fig. 4a–c). Moreover, this noncatalytic function of Polκ was also observed when the DPC was placed on the leading or lagging strand template (Extended Data Fig. 4d,e)[57]. Together, these results indicate a noncatalytic function of Polκ in stimulating Rev1–Polζ-mediated extension across a major groove DPC lesion.

To further validate this noncatalytic function, we purified a Polκ C-terminal fragment devoid of the catalytic domain (Polκ C-ter) (Fig. 4c). Addition of Polκ C-ter restored extension past the lesion, albeit not as efficiently as the full-length protein (Fig. 4d,e, lanes 11–15 versus lanes 16–20). Thus, through its long disordered C-terminal region, Polκ can stimulate Polζ-mediated extension across the DPC.

Interestingly, addition of PIP1 mutant but not PIP2 mutant Polκ restored efficient TLS across DPCs (Extended Data Fig. 4f). Moreover, addition of UBZ1 mutant but not UBZ2 mutant Polκ rescued the TLS defect (Extended Data Figs. 4g and 3e). Thus, in contrast to Polκ's catalytic function, which is independent of Rev1, Polκ's noncatalytic function in DPC bypass requires binding to Rev1 (through RIR), ubiquitin (through UBZ2) and PCNA (through PIP2) (Discussion).

https://doi.org/10.1038/s41594-024-01395-3

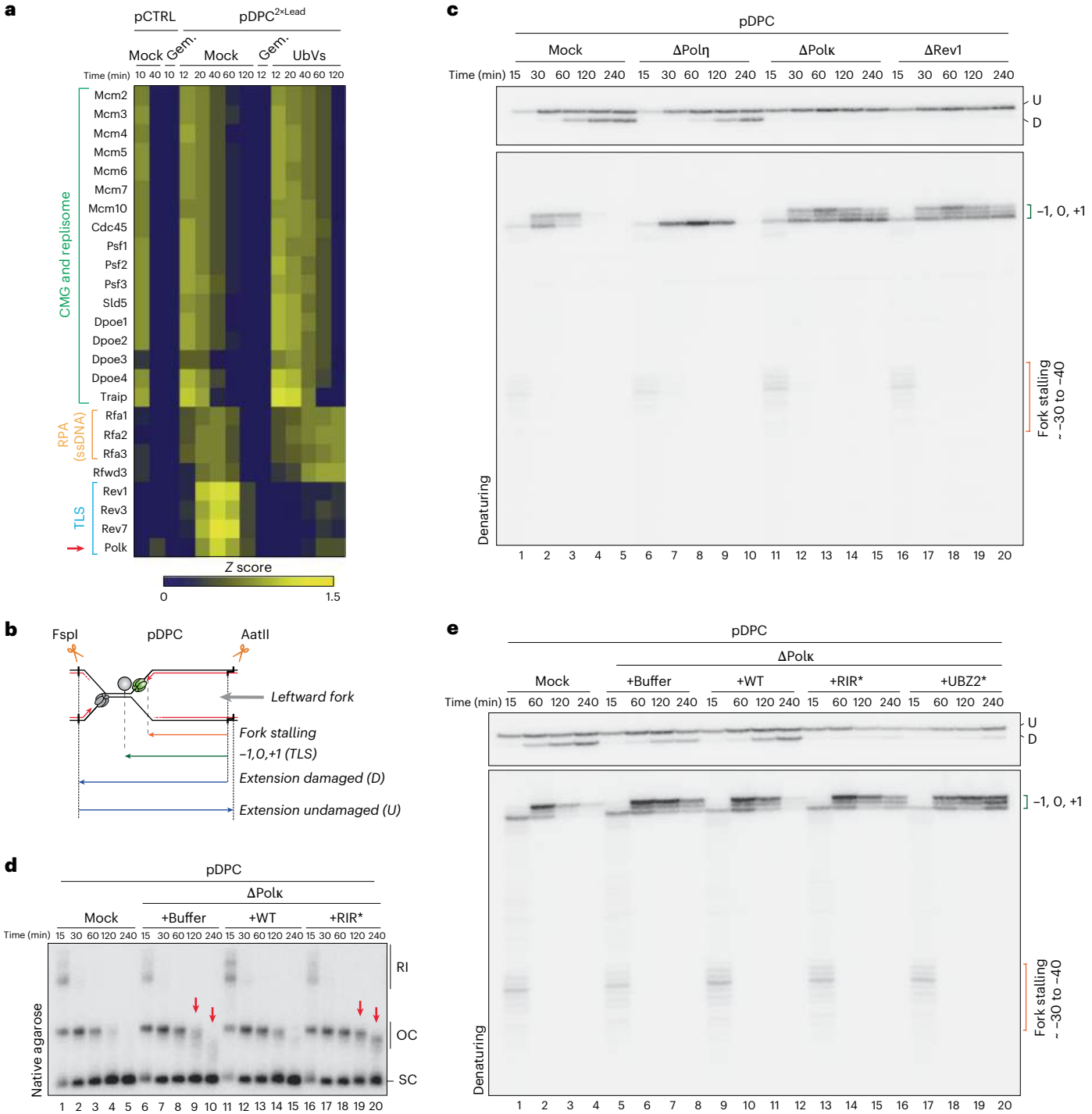

Fig. 3 | Polκ's RIR is required for the bypass of a major groove DPC lesion. **a**, Heat map displaying the mean of the *z*-scored $\log_2$(LFQ intensity) obtained from four biochemical replicates of pCTRL and pDPC$^{2\times Lead}$. Geminin was added to block DNA replication where indicated. Ubiquitin-vinyl sulfone (UbVS) was added where indicated to block ubiquitin recycling and deplete the pool of free ubiquitin from the extracts. These data were originally published in a previous study[56]. **b**, Scheme displaying the nascent leading strand and extension products generated upon FspI and AatII digestion of pDPC. Double digestion generates shorter damaged and longer undamaged extension products, which can be resolved on a denaturing polyacrylamide gel. The CMG helicase is depicted in green, while the crosslinked M.HpaII is depicted in gray. **c**, pDPC was replicated in egg extracts in mock, Polη-depleted, Polκ-depleted or Rev1-depleted extracts. Reaction samples were digested with FspI and AatII, followed by separation on a denaturing polyacrylamide gel. The stalling points position in relationship to the DPC are shown in the lower radiograph. The upper radiograph shows the extension products. **d**, Mock and Polκ-depleted egg extracts were used to replicate pDPC. Polκ-depleted extracts were supplemented with buffer, WT Polκ or RIR mutant Polκ. Samples were analyzed as in Fig. 1h. **e**, Mock and Polκ-depleted egg extracts were used to replicate pDPC. Polκ-depleted extracts were supplemented with buffer, WT Polκ or RIR or UBZ2 mutant Polκ. Samples were analyzed as in **c**.

https://doi.org/10.1038/s41594-024-01395-3

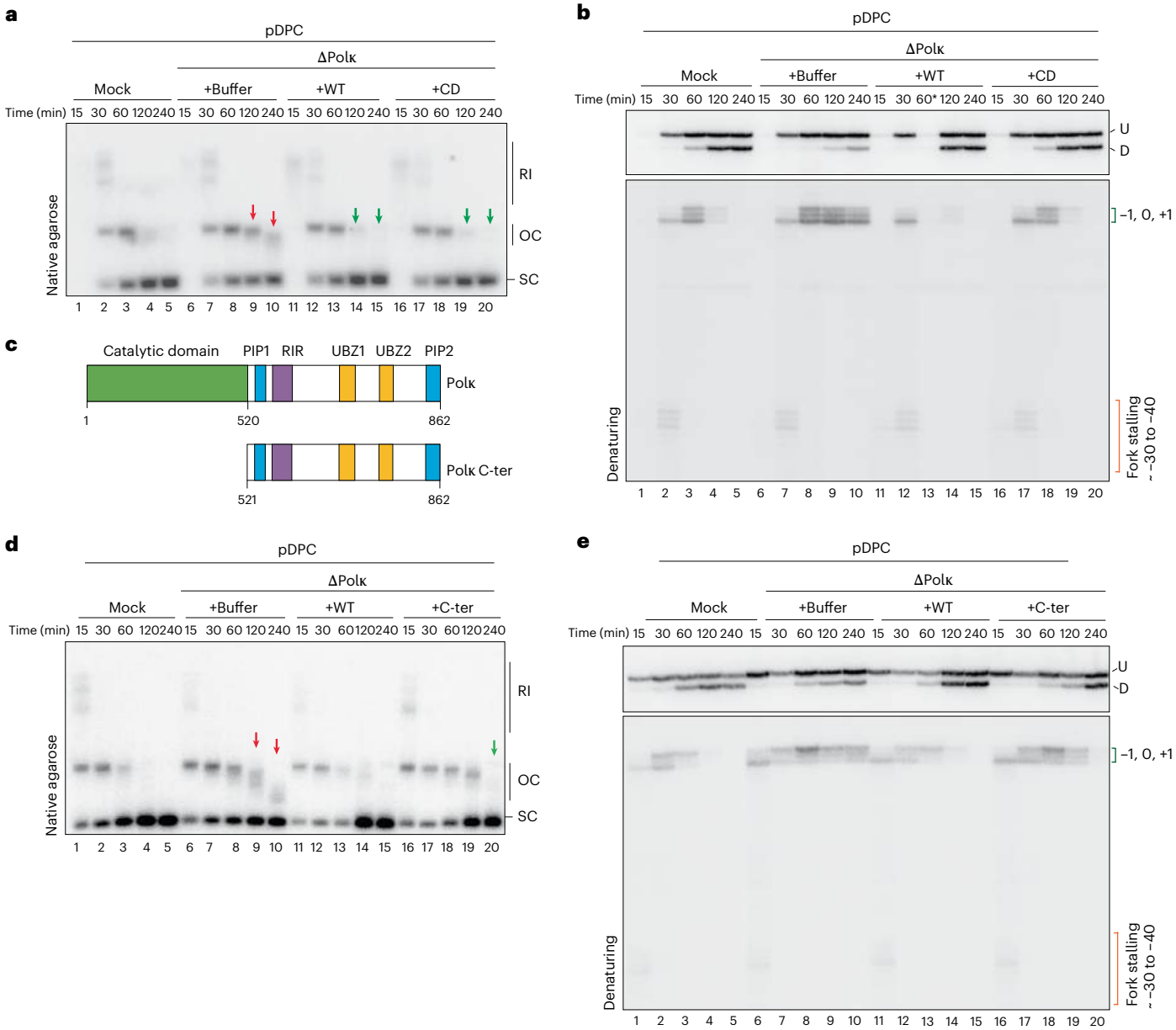

Fig. 4 | Polκ has a noncatalytic function that stimulates Rev1–Polζ-mediated extension across major groove DPC lesions. a, Mock and Polκ-depleted egg extracts were used to replicate pDPC. Polκ-depleted extracts were supplemented with buffer, WT Polκ or CD Polκ. Samples were analyzed as in Fig. 1h. **b**, Samples from **a** were digested with FspI and AatII and separated on a denaturing polyacrylamide gel. Samples were analyzed as in Fig. 3c. The asterisk denotes a sample that was partially lost during DNA extraction (lane 13). **c**, Schematic of *X. laevis* Polκ showing the domain architecture of WT Polκ and Polκ C-ter. **d**, Polκ-depleted extracts were supplemented with buffer, WT Polκ or Polκ C-ter. Samples were analyzed as in Fig. 1h. **e**, Samples from **d** were digested with FspI and AatII and separated on a denaturing polyacrylamide gel. Samples were analyzed as in Fig. 3c.

Polκ stimulates Polζ extension across different DNA lesions

We next investigated whether the noncatalytic function of Polκ is specific to M.HpaII DPCs or whether it could be extended to other DPCs, such as those generated endogenously by HMCES crosslinking[58]. It was recently shown that HMCES crosslinks to AP sites in single-stranded DNA (ssDNA) to protect them from nucleophilic attack and double-strand breaks (DSBs)[58]. HMCES DPCs are endogenous intermediate lesions formed during the repair of interstrand crosslinks formed at an AP site (AP-ICL)[59]. During this process, the NEIL3 glycosylase is recruited to stalled forks and unhooks the AP-ICL by cleaving the *N*-glycosyl bond of the crosslinked site. This generates an AP site on one of the daughter molecules (Fig. 5a, i and ii), which is quickly protected by HMCES[59,60]. HMCES DPCs are then degraded by SPRTN and the resulting peptide–DNA adduct is bypassed by Rev1–Polζ (Fig. 5a, iii)[59,60].

To address whether Polκ also assists Polζ during the bypass of HMCES DPCs, we replicated the AP-ICL plasmid in mock or Polκ-depleted extracts. In the absence of Polκ, permanent stalling at –1 was observed for the leftward-moving fork, indicating that Polκ is required to bypass HMCES peptide–DNA adducts (Fig. 5b, lanes 1–5 versus lanes 6–10, and Extended Data Fig. 5a). This effect was rescued by the addition of both WT and CD Polκ (Fig. 5b, lanes 11–20, and Extended Data Fig. 5a). Thus, Polκ's noncatalytic function is not restricted to the bypass of M.HpaII DPCs but also occurs on other DPCs, such as endogenous DPCs generated by HMCES crosslinking to AP sites.

We next addressed whether Polκ is also able to assist Rev1–Polζ across another type of physiologically relevant DNA lesion. AP sites are intermediate lesions of AP-ICL repair and dependent on Polζ for their bypass[61]. Thus, to stabilize the AP site, we replicated the AP-ICL plasmid

https://doi.org/10.1038/s41594-024-01395-3

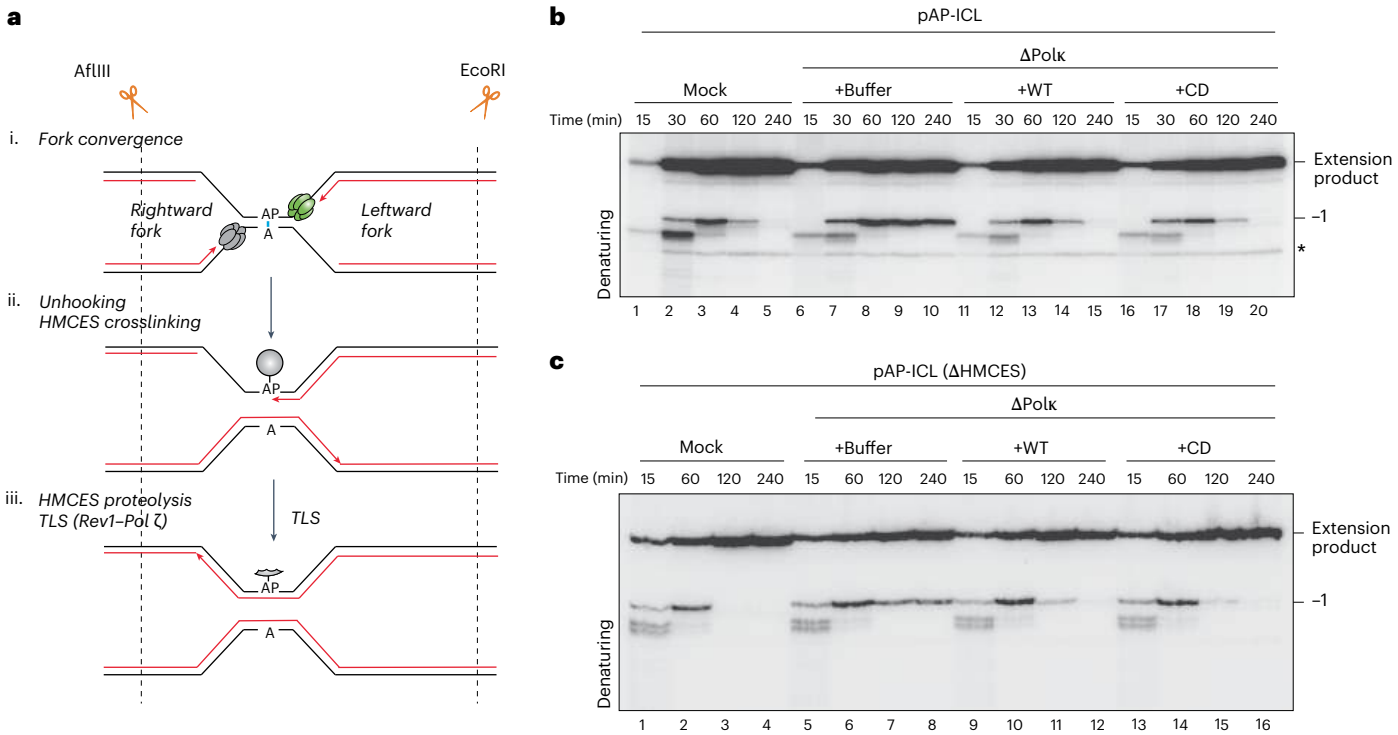

Fig. 5 | Polκ's noncatalytic function stimulates HMCES DPC and AP site bypass. a, Schematic of HMCES DPC formation and proteolysis during replication-coupled AP-ICL repair[59,60]. AflIII and EcoRI allow visualization of stalling points positions relative to the AP-ICL site of the leftward-moving fork. **b**, Mock and Polκ-depleted egg extracts were used to replicate pAP-ICL. Polκ-depleted extracts were supplemented with buffer, WT Polκ or CD Polκ. Samples were subsequently digested with AflIII and EcoRI, followed by separation on a denaturing polyacrylamide gel. Extension products and stalling points position in relationship to the AP-ICL are indicated on the right side of the gel. The asterisk indicates a nonspecific digestion product. **c**, HMCES-depleted extracts were further mock-treated or Polκ-depleted and used to replicate pAP-ICL. Polκ-depleted extracts were supplemented with buffer, WT Polκ or CD Polκ. The samples were analyzed as in **b**.

in the absence of HMCES (Extended Data Fig. 5b,c)[59]. In this setting, Polκ depletion again resulted in permanent stalling at −1 (Fig. 5c, lanes 5–8, and Extended Data Fig. 5d), which was again rescued by the addition of both WT and CD Polκ (Fig. 5c, lanes 9–16, and Extended Data Fig. 5d). Thus, the noncatalytic function of Polκ extends beyond DPCs to other types of Rev1–Polζ-dependent DNA lesions such as AP sites.

Polκ and Rev1–Polζ form a complex on damaged chromatin

Next, we explored the mechanism by which Polκ promotes Polζ-mediated extension. We first hypothesized that Polκ could promote polymerase switching between Polη and Polζ by stimulating the removal of Polη. To test this, we monitored Polκ's function during pDPC replication in the absence of Polη. Unlike Polη depletion, which is permissive to Polζ-mediated bypass (Fig. 6a, lanes 6–10, and Extended Data Fig. 6a)[15], the absence of both Polη and Polκ inhibited TLS across the lesion and nascent strands now permanently stalled at −1 (Fig. 6a, lanes 11–15). This was rescued with WT or CD Polκ (Fig. 6a, lanes 16–25, and Extended Data Fig. 6a), indicating that Polκ assists Polζ catalysis, even in the absence of Polη. These results suggest that Polκ directly stimulates Polζ recruitment and/or activity during TLS and that this function is independent of the prior engagement of another TLS polymerase at the lesion site. Moreover, it indicates that Polκ can assist Polζ not only during the extension but also during the insertion step across a damaged nucleotide.

We previously showed that, upon high-dose UV-C damage, Polκ is de-enriched from damaged chromatin when Rev1–Polζ is depleted from extracts (Fig. 6b)[15], according to chromatin mass spectrometry (CHROMASS) experiments performed in the absence of DNA replication. Because Polκ and Rev1 do not codeplete each other (Extended Data Fig. 3b), this suggests that Polκ may form a complex with Rev1–Polζ on damaged chromatin. To assess the potential interdependency between Polκ and Rev1–Polζ localization to damaged chromatin, we performed a similar CHROMASS experiment to identify proteins whose recruitment depend on either Polκ or Rev1 (ref. 62). Briefly, sperm chromatin was treated with a high dose of UV-C, followed by its incubation in mock, Polκ-depleted or Rev1-depleted egg extracts and analysis by quantitative mass spectrometry (MS) (Fig. 6c, top). This experiment was also performed in the absence of DNA replication to minimize effects arising from uncoupled DNA replication fork structures. Notably, when DNA is irradiated with a high UV-C dose, closely spaced opposing lesions are generated, which trigger the recruitment of TLS polymerases following a first round of nucleotide excision[63]. Accordingly, we observe PCNA ubiquitylation and a robust enrichment of TLS polymerases in the absence of DNA replication (Extended Data Fig. 6b)[15,64].

Consistent with Rev1–Polζ and Polκ forming a complex on damaged DNA, Rev1 depletion led to a significant de-enrichment of Polκ from damaged chromatin (Fig. 6c, *y* axis, Extended Data Fig. 6c and Supplementary Table 2). Similarly, Polκ depletion also led to the de-enrichment of Rev1–Polζ (Fig. 6c, *x* axis, Extended Data Fig. 6d and Supplementary Table 2). Note that Scai, which associates with Rev1–Polζ[64], was also significantly de-enriched in both conditions (Fig. 6c). In addition to Polζ, we noted that many Fanconi anemia (FA) proteins were significantly de-enriched from Polκ-depleted samples (Extended Data Fig. 6d). This was likely caused by a codepletion of the FA complex with the anti-Polκ antibody (Extended Data Fig. 6e,f). Conversely, upon depletion of either Rev1 or Polκ, we observed the enrichment of Polη and its interactor Wrnip1 (refs. 65,66), as well as proteins involved in DSB repair, such as Rnf168 and 53bp1 (Fig. 6c). This suggests that, in the absence of either Polκ or Rev1–Polζ, gap-filling synthesis across certain UV lesions is disrupted (for example, UV-induced 6–4 photoproducts),

https://doi.org/10.1038/s41594-024-01395-3

which leads to the accumulation of Polη on chromatin and the formation of DSBs. Alternatively, the accumulation of 53bp1 could be linked to the formation of large ssDNA gaps that form when TLS is inhibited and the described role of 53bp1 in regulating the balance between TLS and TS[67].

To validate our CHROMASS results, we assessed protein recruitment to UV-damaged sperm chromatin by immunoblotting upon Rev1 or Polκ depletion. As controls, we also depleted Polη or Rfwd3, which regulates PCNA ubiquitylation and TLS polymerase recruitment to lesion sites[15]. Consistent with this, Rfwd3 depletion led to impaired PCNA ubiquitylation and de-enrichment of Polη, Rev1–Polζ, and Polκ to UV-treated chromatin compared to the control reaction (Fig. 6d, lanes 4–8 versus lanes 10–14). Confirming the CHROMASS results, the enrichment of Rev1–Polζ was also impaired in the absence of Polκ (Fig. 6d, lanes 4 and 5 versus lanes 10 and 11). Similarly, the recruitment of Polκ was reduced in the absence of Rev1 (Fig. 6d, lanes 4–7

Fig. 6 | Polκ and Rev1–Polζ form a stable complex on damaged DNA. a, Mock, Polη-depleted or Polη-depleted and Polκ-depleted egg extracts were used to replicate pDPC. Polκ-depleted extracts were supplemented with buffer, WT Polκ or CD Polκ. Samples were subsequently digested with FspI and AatII and analyzed as in Fig. 3c. **b**, CHROMASS analysis of protein recruitment to UV-treated sperm chromatin in mock or Rev1-depleted extracts. Note that this experiment was performed in the absence of DNA replication. The volcano plot illustrates the difference in abundance of proteins between the two sample conditions (*x* axis), plotted against the *P* value resulting from two-tailed Student's two-sample *t*-testing (*y* axis). Proteins significantly downregulated or upregulated (FDR < 5%) in Rev1-depleted reactions are represented in red or blue, respectively ($n = 4$ biochemical replicates). FDR < 5% corresponds to a *q* value < 0.05. Different isoforms of the same protein can be detected (for example, Rev1). These data were originally published in a previous study[15]. **c**, Top, schematic of CHROMASS. Bottom, graph illustrating protein recruitment to UV-treated sperm chromatin in the presence or absence of Rev1 or Polκ, as determined by CHROMASS analysis (Supplementary Table 2). This experiment was performed in the absence of DNA replication. Red dots (bottom-left quadrant) indicate the proteins that were significantly de-enriched on sperm chromatin in the absence of Rev1 and Polκ. Blue dots (top-right quadrant) indicate the proteins that were significantly enriched on sperm chromatin in the absence of Rev1 and Polκ. Orange dots indicate the proteins that were significantly de-enriched on sperm chromatin in the absence of Polκ ($n = 4$ biochemical and $n = 8$ technical replicates; significance was determined by two-tailed Student's two-sample *t*-testing, with a permutation-based FDR control ($s_0 = 0.5$) to ensure a *q* value < 0.05. Note that different isoforms of the same protein can sometimes be detected. **d**, Sperm chromatin was either untreated or treated with 2,000 J m^{-2} of UV-C and then added to nonreplicating mock, Polη-depleted, Polκ-depleted, Rev1-depleted or Rfwd3-depleted extracts. Chromatin was isolated and the associated proteins were blotted with the indicated antibodies. Red dots correspond to PCNA ubiquitylation (monoubiquitin, diubiquitin and triubiquitin); the gray dot corresponds to monosumoylated PCNA[15]. **e**, Sperm chromatin was either untreated or treated with 2,000 J m^{-2} of UV-C and added to nonreplicating Polκ-depleted extracts. Polκ-depleted extracts were supplemented with buffer, WT Polκ or CD Polκ. Chromatin was isolated and the associated proteins were blotted with the indicated antibodies as in **d**.

versus lanes 10–13). The interdependency between Polκ and Rev1–Polζ was also observed during DNA replication following the treatment of sperm chromatin with low-dose UV-C (Extended Data Fig. 6g) and when monitoring protein recruitment to pDPC by plasmid pulldown (Extended Data Fig. 6h). Moreover, although Rev1–Polζ is not involved in the bypass of the minor groove adduct (Fig. 2c), we could still detect its enrichment on p3d-Phen-A, which was also partially dependent on Polκ (Extended Data Fig. 6i). Thus, the Rev1–Polζ–Polκ complex appears to form during TLS irrespectively of the DNA lesion. In contrast, Polη enrichment to damaged chromatin was independent of either Rev1 or Polκ; conversely, the absence of Polη did not impact Rev1–Polζ or Polκ recruitment (Fig. 6d). Rev1–Polζ enrichment could be restored by the addition of WT or CD Polκ to Polκ-depleted extracts (Fig. 6e). Together, these results suggest that Polκ and Rev1–Polζ form a stable complex on damaged DNA, independently of Polη.

Catalytic and noncatalytic functions of Polκ in human cells

To assess the functional importance of Polκ in human cells, we constructed a knockout (KO) and complementation system in U2OS Flp-In T-REx cells. This system allows for stable doxycycline-inducible expression from the *FRT* locus. We generated U2OS *POLK*-KO cells (Extended Data Fig. 7a, clone 1.10) and stably complemented the cells with Venus-tagged WT or CD Polκ (Extended Data Fig. 7b).

As expected, U2OS *POLK*-KO cells were hypersensitive to both illudin S and cisplatin as shown by a colony formation assay (Fig. 7a–d)[34–36,38]. The illudin S hypersensitivity was significantly suppressed by the expression of WT but not CD Polκ (Fig. 7a,b), supporting the requirement of Polκ's catalytic activity for the bypass of illudin S-induced minor groove lesions. In contrast, while the cisplatin sensitivity observed in *POLK*-KO cells was only partially suppressed by the expression of Polκ, it was suppressed equally well by WT or CD Polκ (Fig. 7c,d). This observation supports Polκ's function in cisplatin tolerance that is independent of its catalytic activity.

Discussion

Polκ has the distinct ability among eukaryotic polymerases to bypass minor groove DNA adducts. Here, we study for the first time the bypass mechanism of a minor groove DNA lesion using an extract system that recapitulates DNA replication and TLS. We demonstrate that bypass of a minor groove DNA lesion is exquisitely dependent on Polκ's catalytic activity, validating previous observations made with purified enzymes. Strikingly, we also uncover a noncatalytic function of Polκ during TLS that is required for Polζ-mediated extension past AP sites and major groove DNA lesions. Whereas Polκ's noncatalytic function in TLS requires an interaction with Rev1, Polκ's catalytic function is independent of Rev1. Thus, Polκ serves multiple functions during TLS, which are differentially regulated through its C-terminal disordered region.

Polκ and minor groove DNA lesions

Polκ is the only vertebrate DNA polymerase shown to synthesize across minor groove DNA lesions in vitro but direct evidence of this process in a physiological context was lacking. Using *Xenopus* egg extracts, we show that Polκ is essential to bypass p3d-Phen-A (Fig. 1). In the absence of Polκ, nascent strands remained stalled at the lesion (Fig. 1i), indicating that no other DNA polymerase could compensate for Polκ's absence. This is consistent with the structural features of Polκ, where the unique conformation of the PAD opens its catalytic core toward the minor groove of DNA[28]. Moreover, Polκ contains a unique N-clasp, which contributes to stabilizing the incoming template DNA. In accordance, our base-editor screen suggested that point substitutions in the N-clasp and PAD increase cellular sensitivity to illudin S (Fig. 1b). This

Fig. 7 | Molecular models of Polκ's catalytic and noncatalytic functions during TLS. a,**b**, Colony formation assay with illudin S. U2OS parental cells, *POLK*-KO cells and *POLK*-KO cells stably expressing Venus–WT Polκ or Venus–CD Polκ were seeded at low density and cells expressing Venus–WT Polκ or Venus–CD Polκ were induced with 20 ng ml^{-1} doxycycline. Cells were grown in the presence or absence of 31.25 pg ml^{-1} illudin S and formed colonies were stained and quantified. Examples of images (**a**) and quantification (**b**) are shown. The survival in illudin S represents the average number of colonies at 31.25 pg ml^{-1} illudin S normalized to the untreated condition. Individual data points, means and s.d. values from three independent experiments are plotted. One-way ANOVA with Tukey's multiple-comparisons test was performed and *P* values for the indicated comparisons are shown. **c**,**d**, Colony formation assay with cisplatin. Examples of images (**c**) and quantification (**d**) of a colony formation assay performed as in **a**,**b** but treated with 1 µM cisplatin. **e**,**f**, Composite molecular models of the catalytic (**e**) and noncatalytic (**f**) functions of Polκ during TLS. Models were generated by combining structure predictions from AlphaPulldown[77] and AlphaFold2 (ref. 78), as described in the Methods. During its catalytic function (**e**), Polκ can interact with PCNA monomers through its PIP1 or PIP2 domains, bringing its catalytic domain into close proximity with the DNA substrate. The long flexible Polκ C-terminal region additionally allows Polκ to interact with a monoubiquitinated PCNA through its UBZ2 domain. During its noncatalytic function (**f**), Polκ can bind Rev1 through its RIR domain; the UBZ2 and PIP2 domains are able to bind to monoubiquitinated PCNA thanks to the long flexible Polκ C-terminal region. Notably, whilst the Polκ RIR domain is bound to Rev1, the PIP1 domain is positioned such that it would be unable to interact with monoubiquitylated PCNA. Note that the existence of a Rev1–Polζ–Polκ complex is inferred from a previous study[47] and data presented in this manuscript.

https://doi.org/10.1038/s41594-024-01395-3

is likely because of the impaired ability of these mutants in bypassing minor groove DNA adducts induced by illudin S.

We further provide the regulatory mechanisms underlying Polκ's catalytic function across the minor groove DNA lesion. Previous in vitro studies reported that Polκ's interaction with PCNA through its PIP1 domain was required for Polκ's catalytic activity, whereas PIP2 was dispensable[54,55]. Our base-editor screen showed that gRNAs targeting PIP1 but not PIP2 increased the sensitivity to illudin S, reinforcing that PIP1 mediates the primary Polκ–PCNA interaction required for DNA synthesis (Fig. 1b). However, our work with extracts suggests that PIP2 also contributes to Polκ's function. We found that while PIP1 or PIP2 mutants exhibited mildly affected catalytic function, PIP1 and PIP2 double

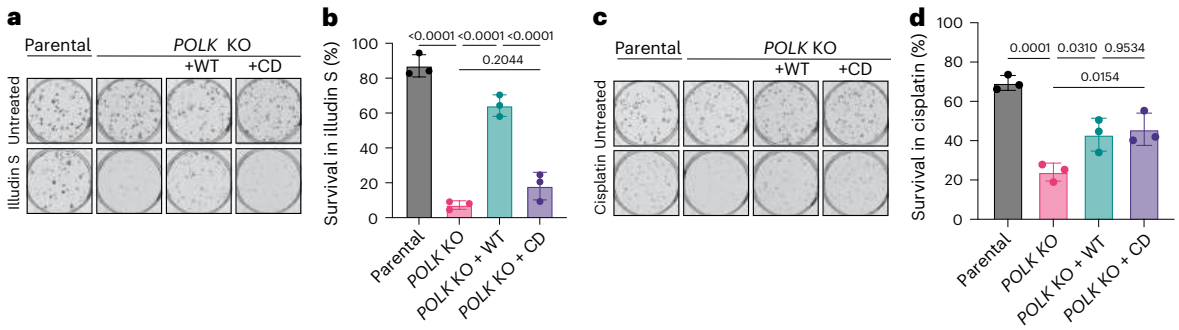

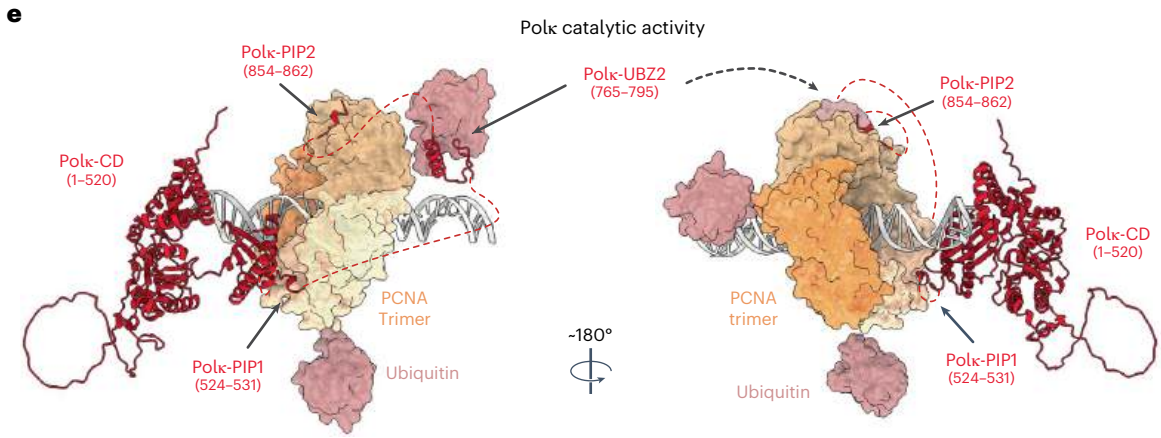

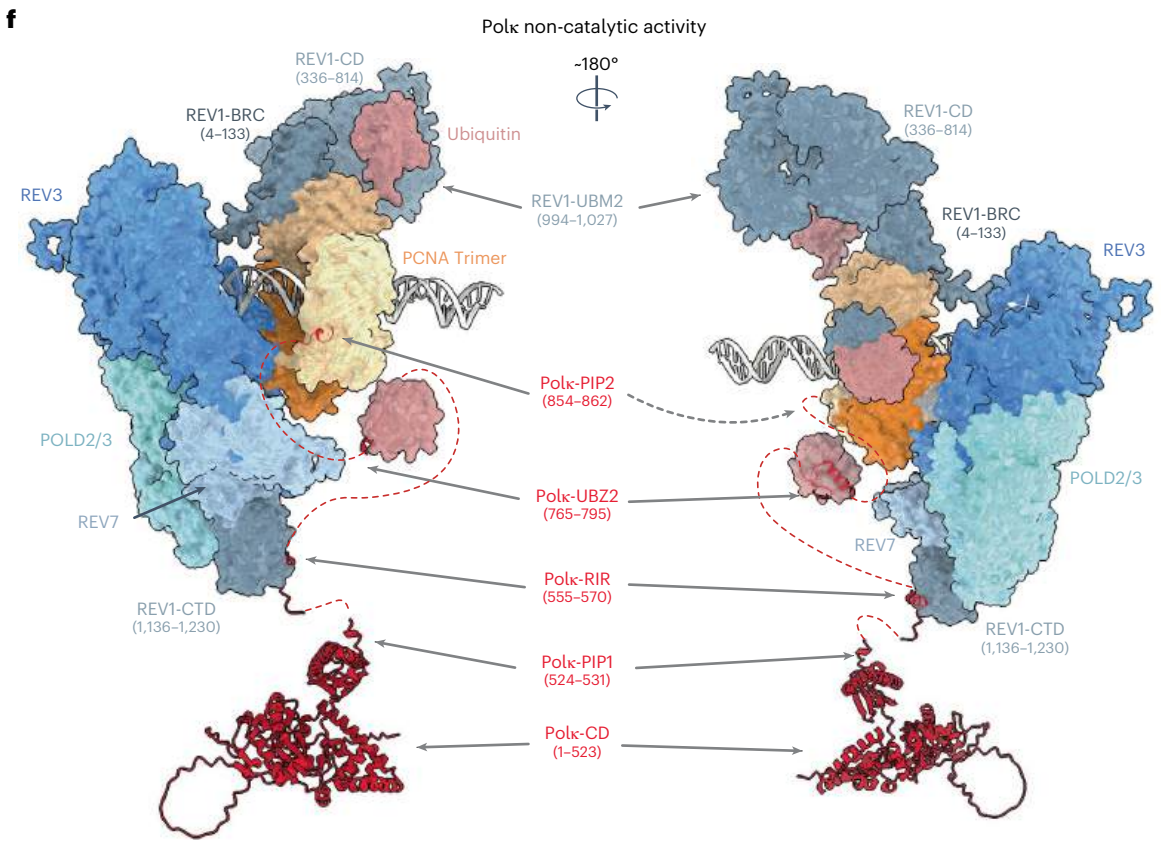

mutants exhibited severely impaired lesion bypass (Fig. 2d), implying that PIP1 and PIP2 can partially compensate for each other during catalysis. Consistent with our data, a composite model of the catalytic complex suggests that both PIPs are capable of binding DNA-loaded PCNA simultaneously (Fig. 7e), which may increase Polκ's association with PCNA during lesion bypass. In this scenario, we envision that each PIP binds successively; PIP2 initially binds a free PCNA molecule within the trimer, followed by PIP1 binding to a second PCNA molecule, effectively locking Polκ's catalytic site on the damaged template.

In addition to PCNA-binding domains, Polκ contains an RIR[53,68]. Rev1 was shown to act as a scaffolding protein that recruits Y-family TLS polymerases to damaged sites[68]. However, we show that Polκ-dependent bypass of the minor groove adduct does not require Rev1 or Rev1 binding (Fig. 2b,c). Instead, Polκ's interaction with ubiquitylated PCNA (through PIP1, PIP2 and UBZ2) appears to be sufficient for Polκ-mediated synthesis (Fig. 7e).

Together, our work supports the notion that Polκ is the vertebrate translesion polymerase specialized in bypassing minor groove DNA lesions.

Polκ's noncatalytic function in TLS

We show that Polκ, through its RIR, stimulates Polζ-mediated extension across different DNA lesions in a process independent of Polκ's catalytic activity (Figs. 3–5). In fact, even a truncated Polκ lacking its catalytic domain was able to stimulate Polζ-mediated bypass, albeit not as efficiently as the full-length protein (Fig. 4d,e). This suggests that most of the stimulatory functions are driven by Polκ's C-terminal domains, which interact with ubiquitylated PCNA and Rev1 (Fig. 7f). The reduced rescue efficiency by the Polκ C-terminal fragment could be attributed to its highly disordered structure, which may reduce the stability of the protein fragment compared to full-length Polκ.

By superimposing AlphaFold2-generated molecular models of *Xenopus* Rev1–Polζ onto the known Rev1–Polζ structure from yeast[69] and modeling the interactions between Polκ and this complex, we find that the Polκ–Rev1 interaction through the RIR domain is likely mutually exclusive with a PIP1 interaction with PCNA (Fig. 7f). Consistent with this, Polκ's noncatalytic function requires Polκ RIR and PIP2 but is independent of PIP1 (Fig. 3e and Extended Data Fig. 4f). On the basis of our findings that Rev1–Polζ and Polκ recruitment to damaged DNA are reciprocally dependent on each other (Fig. 6), we propose that Polκ uses its multiple interaction domains to stabilize the Rev1–Polζ complex on DNA, promoting Polζ-mediated extension beyond various DNA lesions (Fig. 7f). This complex may serve as the last-resort TLS complex, functioning only after failed attempts by Y-family polymerases to bypass a lesion (that is, Polη, Polκ, Rev1 or Polι). These lesions could include those across which Y-family polymerases can insert but not extend (for example, 6–4 photoproducts or M.HpaII DPCs), as well as lesions unsuited for Y-family polymerase insertion. Notably, our results build upon a previous structural study that showed the formation of a stable Rev1–Rev3–Rev7–Polκ quaternary complex in vitro[47], now highlighting the functional relevance of this complex.

Interestingly, in addition to its catalytic function across minor groove DNA lesions, Polκ possesses extension activity past mismatched bases in vitro[70,71]. The formation of a Rev1–Polζ–Polκ complex would enable the recruitment of two distinct polymerases with extension activity to the same DNA lesion. Although we only observe the stimulation of Polζ by Polκ, it is tempting to speculate that the opposite might also occur on DNA lesions that Polζ is unable to bypass. This arrangement would provide a safeguarding mechanism, ensuring that, if one polymerase is unable to extend past the DNA lesion, the other polymerase could quickly replace it and extend beyond the damage. Together, our data reveal both catalytic and noncatalytic functions of Polκ during TLS and demonstrate the specific roles of its different interaction domains for each function.

Polκ's role in NER

Polκ was shown to participate in the DNA synthesis step of NER, both in human cells irradiated with UV-C[37,41] and in *Xenopus* egg extracts during the repair of a trimethylene ICL[36]. A recent study showed that the participation of TLS polymerases during NER also includes Rev1, Polη and Polι when closely spaced opposing lesions are generated following high doses of UV-C[63]. Accordingly, we show that Polη, Rev1–Polζ and Polκ are all recruited to chromatin treated with high-dose UV-C in the absence of DNA replication (Fig. 6). Ultimately, the nature of the lesion dictates which TLS polymerase is used for its bypass. A previous study showed that the bypass of a trymethylene ICL during NER required Polκ's catalytic function, whereas Polκ's binding to Rev1 was dispensable[36]. In light of our findings, we propose that this is attributed to Polκ's catalytic role in bypassing the minor groove trimethylene adduct, rather than to a specific regulation of Polκ by NER.

Role of Rev1 in Y-family TLS regulation

Y-family TLS polymerases feature long, flexible C-terminal ends that harbor multiple interaction domains with PCNA, ubiquitin and Rev1. Existing models propose that PCNA ubiquitylation facilitates the recruitment of TLS polymerases to sites of DNA lesions[6–8,72]. Alternatively, Rev1 acts as a scaffold, enabling the recruitment of TLS polymerases to damaged sites regardless of PCNA ubiquitylation status[19,68]. Thus, two modes of TLS polymerase recruitment coexist but the precise interplay and conditions determining the relevance of each pathway remain unknown. In our study, we showed that binding of Polκ to ubiquitylated PCNA is likely sufficient for targeting its catalytic function (Fig. 2). In contrast, Rev1 regulates Polκ's noncatalytic function in stimulating Polζ extension (Fig. 3d,e). Thus, rather than acting as a general recruitment platform for Y-family polymerases, Rev1 appears to govern the assembly of specialized TLS subcomplexes. We envision that these complexes may form on DNA irrespectively of the DNA lesion but the lesion type ultimately dictates the TLS complex used to bypass it. Like Polκ, Polη and Polι also contain RIRs of unclear importance, prompting speculation that Rev1 may similarly regulate unknown functions of these polymerases.

Polκ's function in mammalian cells

Consistent with Polκ's unique function in replicating across a minor groove DNA adduct, *POLK*-KO cells exhibit severe sensitivity to minor-groove-inducing agents[35,36], which we show here is dependent on Polκ's catalytic activity (Fig. 7a,b). Intriguingly, *POLK*-KO cells are also sensitive to other DNA-damaging agents, such as UV and cisplatin, which induce lesions on the major groove of DNA that require Polζ-mediated extension for bypass[20,22,35,37]. Our study revealed that the sensitivity to cisplatin observed in the absence of Polκ could be partially restored to the same extent with WT or CD Polκ (Fig. 7c,d). Hence, we propose that the sensitivity of *POLK*-KO cells to UV and cisplatin is attributed to the noncatalytic function of Polκ, facilitating Rev1–Polζ-dependent TLS. Notably, *POLK*-KO cells have also been reported to be sensitive to oxidative agents, such as potassium bromate, which generates AP sites and HMCES DPCs[35]. This sensitivity may also be linked to Polκ's noncatalytic role across AP sites or HMCES DPCs, as we report here (Fig. 5).

Unlike *POLK*-KO cells, *REV3*$^{-/-}$ mouse embryonic stem cells are not viable[73], which suggests that Polζ possesses functions independent of Polκ. Interestingly, Rev3 also has a role beyond TLS by facilitating DNA replication through heterochromatic regions[74], which could account for its essential role.

Emerging strategies in cancer therapy include the development of TLS inhibitors, which may enhance tumor sensitivity to first-line chemotherapeutics[75,76]. Notably, our results emphasize the potential benefit of targeting specific functional domains within Y-family polymerases, such as the Polκ–Rev1 interaction. This targeted approach may selectively sensitize cancer cells to genotoxic agents.

Online content

Any methods, additional references, Nature Portfolio reporting summaries, source data, extended data, supplementary information, acknowledgements, peer review information; details of author contributions and competing interests; and statements of data and code availability are available at https://doi.org/10.1038/s41594-024-01395-3.

References

1. Ling, H., Boudsocq, F., Woodgate, R. & Yang, W. Crystal structure of a Y-family DNA polymerase in action: a mechanism for error-prone and lesion-bypass replication. *Cell* **107**, 91–102 (2001).
2. Goodman, M. F. & Woodgate, R. Translesion DNA polymerases. *Cold Spring Harb. Perspect. Biol.* **5**, a010363 (2013).
3. Cortez, D. Replication-coupled DNA repair. *Mol. Cell* **74**, 866–876 (2019).
4. Saldivar, J. C., Cortez, D. & Cimprich, K. A. The essential kinase ATR: ensuring faithful duplication of a challenging genome. *Nat. Rev. Mol. Cell Biol.* **18**, 622–636 (2017).
5. Friedberg, E. C., Wagner, R. & Radman, M. Specialized DNA polymerases, cellular survival, and the genesis of mutations. *Science* **296**, 1627–1630 (2002).
6. Hoege, C., Pfander, B., Moldovan, G.-L., Pyrowolakis, G. & Jentsch, S. RAD6-dependent DNA repair is linked to modification of PCNA by ubiquitin and SUMO. *Nature* **419**, 135–141 (2002).
7. Stelter, P. & Ulrich, H. D. Control of spontaneous and damage-induced mutagenesis by SUMO and ubiquitin conjugation. *Nature* **425**, 188–191 (2003).
8. Watanabe, K. et al. Rad18 guides Polη to replication stalling sites through physical interaction and PCNA monoubiquitination. *EMBO J.* **23**, 3886–3896 (2004).
9. Sale, J. E., Lehmann, A. R. & Woodgate, R. Y-family DNA polymerases and their role in tolerance of cellular DNA damage. *Nat. Rev. Mol. Cell Biol.* **13**, 141–152 (2012).
10. Johnson, R. E., Prakash, S. & Prakash, L. Efficient bypass of a thymine–thymine dimer by yeast DNA polymerase, Polη. *Science* **283**, 1001–1004 (1999).
11. Masutani, C., Kusumoto, R., Iwai, S. & Hanaoka, F. Mechanisms of accurate translesion synthesis by human DNA polymerase η. *EMBO J.* **19**, 3100–3109 (2000).
12. McCulloch, S. D. et al. Preferential *cis–syn* thymine dimer bypass by DNA polymerase η occurs with biased fidelity. *Nature* **428**, 97–100 (2004).
13. Johnson, R. E., Washington, M. T., Haracska, L., Prakash, S. & Prakash, L. Eukaryotic polymerases ι and ζ act sequentially to bypass DNA lesions. *Nature* **406**, 1015–1019 (2000).
14. Lee, Y.-S., Gregory, M. T. & Yang, W. Human Pol ζ purified with accessory subunits is active in translesion DNA synthesis and complements Pol η in cisplatin bypass. *Proc. Natl Acad. Sci. USA* **111**, 2954–2959 (2014).
15. Gallina, I. et al. The ubiquitin ligase RFWD3 is required for translesion DNA synthesis. *Mol. Cell* **81**, 442–458 (2021).
16. Gibbs, P. E. M., McDonald, J., Woodgate, R. & Lawrence, C. W. The relative roles in vivo of *Saccharomyces cerevisiae* Pol η, Pol ζ, Rev1 protein and Pol32 in the bypass and mutation induction of an abasic site, T–T (6–4) photoadduct and T–T *cis–syn* cyclobutane dimer. *Genetics* **169**, 575–582 (2005).
17. Hicks, J. K. et al. Differential roles for DNA polymerases η, ζ, and REV1 in lesion bypass of intrastrand versus interstrand DNA cross-links. *Mol. Cell. Biol.* **30**, 1217–1230 (2010).
18. Yoon, J.-H., Prakash, L. & Prakash, S. Error-free replicative bypass of (6–4) photoproducts by DNA polymerase ζ in mouse and human cells. *Genes Dev.* **24**, 123–128 (2010).
19. Guo, C. et al. REV1 protein interacts with PCNA: significance of the REV1 BRCT domain in vitro and in vivo. *Mol. Cell* **23**, 265–271 (2006).
20. Martin, S. K. & Wood, R. D. DNA polymerase ζ in DNA replication and repair. *Nucleic Acids Res.* **47**, 8348–8361 (2019).
21. Acharya, N., Johnson, R. E., Pagès, V., Prakash, L. & Prakash, S. Yeast Rev1 protein promotes complex formation of DNA polymerase ζ with Pol32 subunit of DNA polymerase δ. *Proc. Natl Acad. Sci. USA* **106**, 9631–9636 (2009).
22. Budzowska, M., Graham, T. G. W., Sobeck, A., Waga, S. & Walter, J. C. Regulation of the Rev1–Pol ζ complex during bypass of a DNA interstrand cross-link. *EMBO J.* **34**, 1971–1985 (2015).
23. Edmunds, C. E., Simpson, L. J. & Sale, J. E. PCNA ubiquitination and REV1 define temporally distinct mechanisms for controlling translesion synthesis in the avian cell line DT40. *Mol. Cell* **30**, 519–529 (2008).
24. Gerlach, V. L., Feaver, W. J., Fischhaber, P. L. & Friedberg, E. C. Purification and characterization of Polκ, a DNA polymerase encoded by the human *DINB1* gene. *J. Biol. Chem.* **276**, 92–98 (2001).
25. Ogi, T., Kato, T. Jr, Kato, T. & Ohmori, H. Mutation enhancement by DINB1, a mammalian homologue of the *Escherichia coli* mutagenesis protein dinB. *Genes Cells* **4**, 607–618 (1999).
26. Choi, J.-Y., Angel, K. C. & Guengerich, F. P. Translesion synthesis across bulky N^2-alkyl guanine DNA adducts by human DNA polymerase κ. *J. Biol. Chem.* **281**, 21062–21072 (2006).
27. Jarosz, D. F., Godoy, V. G., Delaney, J. C., Essigmann, J. M. & Walker, G. C. A single amino acid governs enhanced activity of DinB DNA polymerases on damaged templates. *Nature* **439**, 225–228 (2006).
28. Jha, V., Bian, C., Xing, G. & Ling, H. Structure and mechanism of error-free replication past the major benzo[a]pyrene adduct by human DNA polymerase κ. *Nucleic Acids Res.* **44**, 4957–4967 (2016).
29. Jha, V. & Ling, H. 2.0 Å resolution crystal structure of human Polκ reveals a new catalytic function of N-clasp in DNA replication. *Sci Rep.* **8**, 15125 (2018).
30. Ogi, T., Shinkai, Y., Tanaka, K. & Ohmori, H. Polκ protects mammalian cells against the lethal and mutagenic effects of benzo[a]pyrene. *Proc. Natl Acad. Sci. USA* **99**, 15548–15553 (2002).
31. Malvezzi, S. et al. Mechanism of RNA polymerase II stalling by DNA alkylation. *Proc. Natl Acad. Sci. USA* **114**, 12172–12177 (2017).
32. Takeiri, A. et al. In vivo evidence that DNA polymerase κ is responsible for error-free bypass across DNA cross-links induced by mitomycin C. *DNA Repair* **24**, 113–121 (2014).
33. Tanasova, M. & Sturla, S. J. Chemistry and biology of acylfulvenes: sesquiterpene-derived antitumor agents. *Chem. Rev.* **112**, 3578–3610 (2012).
34. Casimir, L., Zimmer, S., Racine-Brassard, F., Jacques, P.-É. & Maréchal, A. The mutational impact of illudin S on human cells. *DNA Repair* **122**, 103433 (2023).
35. Olivieri, M. et al. A genetic map of the response to DNA damage in human cells. *Cell* **182**, 481–496 (2020).
36. Williams, H. L., Gottesman, M. E. & Gautier, J. Replication-independent repair of DNA interstrand crosslinks. *Mol. Cell* **47**, 140–147 (2012).
37. Ogi, T. & Lehmann, A. R. The Y-family DNA polymerase κ (Pol κ) functions in mammalian nucleotide-excision repair. *Nat. Cell Biol.* **8**, 640–642 (2006).
38. Spanjaard, A. et al. Division of labor within the DNA damage tolerance system reveals non-epistatic and clinically actionable targets for precision cancer medicine. *Nucleic Acids Res.* **50**, 7420–7435 (2022).
39. Johnson, R. E., Prakash, S. & Prakash, L. The human *DINB1* gene encodes the DNA polymerase Polθ. *Proc. Natl Acad. Sci. USA* **97**, 3838–3843 (2000).

40. Kanemaru, Y. et al. Catalytic and non-catalytic roles of DNA polymerase κ in the protection of human cells against genotoxic stresses. *Environ. Mol. Mutagen.* **56**, 650–662 (2015).
41. Ogi, T. et al. Three DNA polymerases, recruited by different mechanisms, carry out NER repair synthesis in human cells. *Mol. Cell* **37**, 714–727 (2010).
42. Bétous, R. et al. DNA polymerase κ-dependent DNA synthesis at stalled replication forks is important for CHK1 activation. *EMBO J.* **32**, 2172–2185 (2013).
43. Dall'Osto, M., Pierini, L., Valery, N., Hoffmann, J.-S. & Pillaire, M.-J. A catalytically independent function of human DNA polymerase κ controls the stability and abundance of checkpoint kinase 1. *Mol. Cell. Biol.* **41**, e0009021 (2021).
44. Tonzi, P., Yin, Y., Lee, C. W. T., Rothenberg, E. & Huang, T. T. Translesion polymerase κ-dependent DNA synthesis underlies replication fork recovery. *eLife* **7**, e41426 (2018).
45. Hishiki, A. et al. Structural basis for novel interactions between human translesion synthesis polymerases and proliferating cell nuclear antigen. *J. Biol. Chem.* **284**, 10552–10560 (2009).
46. Vaisman, A. & Woodgate, R. Translesion DNA polymerases in eukaryotes: what makes them tick? *Crit. Rev. Biochem. Mol. Biol.* **52**, 274–303 (2017).
47. Xie, W., Yang, X., Xu, M. & Jiang, T. Structural insights into the assembly of human translesion polymerase complexes. *Protein Cell* **3**, 864–874 (2012).
48. Sangree, A. K. et al. Benchmarking of SpCas9 variants enables deeper base editor screens of *BRCA1* and *BCL2*. *Nat. Commun.* **13**, 1318 (2022).
49. Boudsocq, F. et al. Investigating the role of the little finger domain of Y-family DNA polymerases in low fidelity synthesis and translesion replication. *J. Biol. Chem.* **279**, 32932–32940 (2004).
50. Walter, J., Sun, L. & Newport, J. Regulated chromosomal DNA replication in the absence of a nucleus. *Mol. Cell* **1**, 519–529 (1998).
51. Ogi, T., Kannouche, P. & Lehmann, A. R. Localisation of human Y-family DNA polymerase κ: relationship to PCNA foci. *J. Cell Sci.* **118**, 129–136 (2005).
52. Guo, C., Tang, T.-S., Bienko, M., Dikic, I. & Friedberg, E. C. Requirements for the interaction of mouse Polκ with ubiquitin and its biological significance. *J. Biol. Chem.* **283**, 4658–4664 (2008).
53. Ohashi, E. et al. Identification of a novel REV1-interacting motif necessary for DNA polymerase κ function. *Genes Cells* **14**, 101–111 (2009).
54. Masuda, Y. et al. Different types of interaction between PCNA and PIP boxes contribute to distinct cellular functions of Y-family DNA polymerases. *Nucleic Acids Res.* **43**, 7898–7910 (2015).
55. Lancey, C. et al. Cryo-EM structure of human Pol κ bound to DNA and mono-ubiquitylated PCNA. *Nat. Commun.* **12**, 6095 (2021).
56. Larsen, N. B. et al. Replication-coupled DNA–protein crosslink repair by SPRTN and the proteasome in *Xenopus* egg extracts. *Mol. Cell* **73**, 574–588 (2019).
57. Duxin, J. P., Dewar, J. M., Yardimci, H. & Walter, J. C. Repair of a DNA–protein crosslink by replication-coupled proteolysis. *Cell* **159**, 346–357 (2014).
58. Mohni, K. N. et al. HMCES maintains genome integrity by shielding abasic sites in single-strand DNA. *Cell* **176**, 144–153 (2019).
59. Semlow, D. R., MacKrell, V. A. & Walter, J. C. The HMCES DNA–protein cross-link functions as an intermediate in DNA interstrand cross-link repair. *Nat. Struct. Mol. Biol.* **29**, 451–462 (2022).
60. Semlow, D. R., Zhang, J., Budzowska, M., Drohat, A. C. & Walter, J. C. Replication-dependent unhooking of DNA interstrand cross-links by the NEIL3 glycosylase. *Cell* **167**, 498–511 (2016).
61. Haracska, L. et al. Roles of yeast DNA polymerases δ and ζ and of Rev1 in the bypass of abasic sites. *Genes Dev.* **15**, 945–954 (2001).
62. Räschle, M. et al. Proteomics reveals dynamic assembly of repair complexes during bypass of DNA cross-links. *Science* **348**, 1253671 (2015).
63. Sertic, S. et al. Coordinated activity of Y family TLS polymerases and EXO1 protects non-S phase cells from UV-induced cytotoxic lesions. *Mol. Cell* **70**, 34–47 (2018).
64. Schubert, L. et al. SCAI promotes error-free repair of DNA interstrand crosslinks via the Fanconi anemia pathway. *EMBO Rep.* **23**, e53639 (2022).
65. Yoshimura, A., Kobayashi, Y., Tada, S., Seki, M. & Enomoto, T. WRNIP1 functions upstream of DNA polymerase η in the UV-induced DNA damage response. *Biochem. Biophys. Res. Commun.* **452**, 48–52 (2014).
66. Yuasa, M. S. et al. A human DNA polymerase η complex containing Rad18, Rad6 and Rev1; proteomic analysis and targeting of the complex to the chromatin-bound fraction of cells undergoing replication fork arrest. *Genes Cells* **11**, 731–744 (2006).
67. Chen, D. et al. *BRCA1* deficiency specific base substitution mutagenesis is dependent on translesion synthesis and regulated by 53BP1. *Nat. Commun.* **13**, 226 (2022).
68. Guo, C. et al. Mouse Rev1 protein interacts with multiple DNA polymerases involved in translesion DNA synthesis. *EMBO J.* **22**, 6621–6630 (2003).
69. Malik, R. et al. Structure and mechanism of B-family DNA polymerase ζ specialized for translesion DNA synthesis. *Nat. Struct. Mol. Biol.* **27**, 913–924 (2020).
70. Haracska, L., Prakash, L. & Prakash, S. Role of human DNA polymerase κ as an extender in translesion synthesis. *Proc. Natl Acad. Sci. USA* **99**, 16000–16005 (2002).
71. Washington, M. T., Johnson, R. E., Prakash, L. & Prakash, S. Human *DINB1*-encoded DNA polymerase κ is a promiscuous extender of mispaired primer termini. *Proc. Natl Acad. Sci. USA* **99**, 1910–1914 (2002).
72. Kannouche, P. L., Wing, J. & Lehmann, A. R. Interaction of human DNA polymerase η with monoubiquitinated PCNA: a possible mechanism for the polymerase switch in response to DNA damage. *Mol. Cell* **14**, 491–500 (2004).
73. Lange, S. S., Wittschieben, J. P. & Wood, R. D. DNA polymerase ζ is required for proliferation of normal mammalian cells. *Nucleic Acids Res.* **40**, 4473–4482 (2012).
74. Ben Yamin, B. et al. DNA polymerase ζ contributes to heterochromatin replication to prevent genome instability. *EMBO J.* **40**, e104543 (2021).
75. Wojtaszek, J. L. et al. A small molecule targeting mutagenic translesion synthesis improves chemotherapy. *Cell* **178**, 152–159 (2019).
76. Yamanaka, K., Chatterjee, N., Hemann, M. T. & Walker, G. C. Inhibition of mutagenic translesion synthesis: a possible strategy for improving chemotherapy? *PLoS Genet.* **13**, e1006842 (2017).
77. Yu, D., Chojnowski, G., Rosenthal, M. & Kosinski, J. AlphaPulldown—a python package for protein–protein interaction screens using AlphaFold-Multimer. *Bioinformatics* **39**, btac749 (2023).
78. Jumper, J. et al. Highly accurate protein structure prediction with AlphaFold. *Nature* **596**, 583–589 (2021).
79. Yockey, O. P. et al. Mechanism of error-free DNA replication past lucidin-derived DNA damage by human DNA polymerase κ. *Chem. Res. Toxicol.* **30**, 2023–2032 (2017).
80. Zhang, Z. et al. Structure of monoubiquitinated PCNA: implications for DNA polymerase switching and Okazaki fragment maturation. *Cell Cycle* **11**, 2128–2136 (2012).

[1]Novo Nordisk Foundation Center for Protein Research, University of Copenhagen, Copenhagen, Denmark. [2]Center for Chromosome Stability, Department of Cellular and Molecular Medicine, Faculty of Health and Medical Sciences, University of Copenhagen, Copenhagen, Denmark. [3]Department of Molecular Medicine, University of Padua, Padua, Italy. [4]Division of Cancer Biology, The Institute of Cancer Research, London, UK. [5]Biotech Research and Innovation Centre, Faculty of Health and Medical Sciences, University of Copenhagen, Copenhagen, Denmark. [6]Department of Health Sciences and Technology, ETH Zurich, Zurich, Switzerland. [7]Division of Chemistry and Chemical Engineering, California Institute of Technology, Pasadena, CA, USA. [8]These authors contributed equally: Sara M. Ambjørn, Alberto Carli, Ivo A. Hendriks. ✉e-mail: Julien.duxin@bric.ku.dk

https://doi.org/10.1038/s41594-024-01395-3

Methods

Xenopus egg extracts and DNA replication reactions

Xenopus egg extracts were prepared as described previously[81]. All experiments involving animals were approved by the Danish Animal Experiments Inspectorate and conform to relevant regulatory standards and European guidelines.

For plasmid DNA replication, plasmids were licensed in high-speed supernatant (HSS) at a final concentration of 7.5 ng μl^{-1} for 30 min at room temperature (RT). Replication was initiated by adding two volumes of nucleoplasmic egg extract (NPE). Gap-filling reactions were performed in nonlicensing extracts (extracts that do not support MCM2–MCM7 licensing), where one volume of HSS was premixed with two volumes of NPE before the addition of plasmid DNA (final concentration of 10 ng μl^{-1}). For replication in the presence of LacI, plasmid DNA (150 ng μl^{-1}) was incubated with an equal volume of 12 µM LacI for 1 h before licensing[57]. The ubiquitin E1 inhibitor MLN-7243 (Active Biochem) was supplemented to NPE at a final concentration of 200 µM 10 min before initiating the reaction. To visualize DNA replication intermediates, replication reactions were supplemented with [α-^{32}P] dATP (Perkin Elmer). For each time point, 1 µl of the reaction mixture was added to 5 µl of stop buffer (5% SDS, 80 mM Tris pH 8.0, 0.13% phosphoric acid and 10% Ficoll), followed by the addition of 1 µl of proteinase K (20 mg ml^{-1}) (Roche). The samples were incubated at 37 °C for 1 h and subsequently separated using 0.9% native agarose gel electrophoresis; results were visualized using a phosphor imager. The radioactive signal was quantified using ImageJ (National Institutes of Health).

Preparation of DNA constructs

pDPC and pDPC$^{2\times Lead}$ were prepared as previously described[56]. Additionally, pDPC^{PK} and pDPC$^{ssDNA\text{-}PK}$ were prepared as previously described[15] as pMH^{PK} and pMH$^{ssDNA\text{-}PK}$, respectively. Moreover, pDPC^{Lead} and pDPC^{Lag} were prepared as previously described[57] as pDPC-L$^{Top\ (Lead)}$ and pDPC-L$^{Bot\ (Lag)}$, respectively.

To generate a plasmid containing p3d-Phen-A, we first removed the LacO array from pJSL3 (ref. 82) using the complementary overhangs of the BsrG1 and BsiWI restriction sites. Subsequently, the two Nb.BsrdI nicking sites were removed using mutagenesis. An A located at position 1557 of the plasmid was mutated to a C to remove the first Nb.BsrDI site using the following primers: 5′-CCACGATGCCTGTAGCCATGGCAACAACGTTGC-3′ and 5′- GCAACGTTGTTGCCATGGCTACAGGCATCGTGG-3′. Secondly, a T located at position 1740 of the plasmid was mutated to a C to remove the second Nb.BsrDI site using the following primers: 5′-GGTCTCGCGGTATCATCGCAGCACTGGGGCCAG-3′ and 5′-CTGGCCCCAGTGCTGCGATGATACCGCGAGACC-3′. Afterward, we used the PciI and BsaX1 restriction sites to clone in the oligo 5′-CATGGCTCTTCNACCTCAACTACTTGACCCTCCTCATTCATTGCTTG-3′ to introduce Nt.BspQ1 and Nb.BsrD1 nicking sites. Finally, to generate p3d-Phen-A, the vector was nicked using Nt.BspQ1 and Nb.BsrD1 and ligated with an excess of the following oligo containing 3d-Phen-A at position 15: 5′-ACCTCAACTACTTGACCCTCCTCATT-3′ (ref. 31). pAP-ICL was generated as previously described[60].

Antibodies and immunodepletions

Antibodies to Rev1 (Rev1-N and Rev1-C)[22], Rfwd3 (ref. 15), Polη[15] and HMCES[59] were described previously. Antibodies to Polκ, Rev3 and FancA 2 were raised by New England Peptide by immunizing rabbits with Ac-CPASKKSKPNSSKNTIDRFFK-OH, Ac-CLADLSIPQLD-OH and Ac-CSFKAPDDYDDLFFEPVF-OH, respectively. The antibody to FancA1 was a kind gift of A. Sobeck[83].

To immunodeplete Rev1 from *Xenopus* egg extracts, an equal volume of Protein A Sepharose fast flow (PAS) (GE Health Care) beads was bound to anti-Rev-N or anti-Rev1-C antibodies overnight at 4 °C. The beads were then washed twice with 500 µl of PBS, once with ELB (10 mM HEPES pH 7.7, 50 mM KCl, 2.5 mM $MgCl_2$ and 250 mM sucrose), twice with ELB supplemented with 0.5 M NaCl and twice with ELB. One volume of precleared HSS or NPE was then depleted by mixing with 0.2 volumes of antibody-bound beads and then incubated at RT for 15 min, before being isolated. For HSS, the depletion procedure was performed once with Rev1-N coupled beads and once with Rev1-C coupled beads. For NPE, the depletion procedure was performed twice with Rev1-N coupled beads and once with Rev1-C coupled beads. To immunodeplete Polκ, Polη or Rfwd3 from *Xenopus* egg extracts, one volume of PAS beads was bound to five volumes of affinity-purified antibody (1 mg ml^{-1}). The beads were washed as described above and one volume of precleared HSS or NPE was then depleted by mixing with 0.2 volumes of antibody-bound beads for 15 min at RT. The depletion procedure was performed once for HSS and three times for NPE. For HMCES and Polκ combined depletion, one volume of beads was bound to eight volumes of each affinity-purified antibody (1 mg ml^{-1}). The beads were washed and depletion was performed as described for Polκ immunodepletion.

Immunoprecipitations

For the FancA and Polκ immunoprecipitation experiments, 5 µl of PAS beads were incubated with 10 µg of the respective affinity-purified antibody for 1 h at RT. The Sepharose beads were subsequently washed twice with PBS and three times with IP buffer (10 mM HEPES pH 7.7, 50 mM KCl, 2.5 mM $MgCl_2$ and 0.25% NP-40). Next, 5 µl of NPE was diluted with 20 µl of IP buffer and incubated with antibody-prebound beads for 1 h at RT. The beads were then washed three times with IP buffer and resuspended in 50 µl of 2× Laemmli sample buffer before analysis by western blotting.

Nascent leading-strand analysis

For nascent leading-strand analysis, 3–4 µl of replication reaction was added to ten volumes of transparent stop buffer (50 mM Tris-HCl pH 7.5, 0.5% SDS and 25 mM EDTA). The replication intermediates were purified as previously described[84,85]. The DNA was digested with the indicated restriction enzymes and subsequently supplemented with 0.5 volumes of denaturing PAGE gel loading buffer II (Life technologies). The digested DNA products were separated on a 6% polyacrylamide sequencing gel.

Protein expression and purification

Full-length *Xenopus laevis* Polκ with an N-terminal 6xHis-tag was amplified from pCMV-Sport.ccdb-Polκ[36] and cloned into pET28b (Novagen) using primers A and B and restriction enzymes BamHI and XhoI. *Xenopus* Polκ C-ter with an N-terminal 6xHis-tag was cloned into pET28b using primers B and C and restriction enzymes BamHI and XhoI. Polκ amino acid substitutions were introduced by Quikchange mutagenesis and confirmed by Sanger sequencing.

Plasmids containing WT Polκ, mutant Polκ or Polκ C-ter were transformed into BL21 *Escherichia coli* competent cells. Cells were grown at 37 °C to an optical density of 0.6–0.8 in Luria–Bertani broth and were subsequently induced with 0.5 mM IPTG for 4 h. Bacteria were harvested by centrifugation and resuspended in 20 ml of lysis buffer (50 mM Tris pH 7.5, 300 mM NaCl, 2 mM $MgCl_2$, 1 mM DTT and 1× Roche EDTA-free cOmplete protease inhibitor cocktail). Suspensions were sonicated and cleared by high-speed centrifugation at 15,000 r.p.m. in a F15-8x50cy rotor for 1 h at 4 °C. The soluble fraction was collected and incubated with 2 ml of Ni-NTA Superflow affinity resin (Qiagen), previously equilibrated with lysis buffer, for 2 h at 4 °C. The resin was then washed three times with 20 ml of wash buffer (50 mM Tris pH 7.5, 300 mM NaCl, 2 mM $MgCl_2$, 1 mM DTT, 0,1% Triton-X and 10 mM imidazole). Then, 6xHis-tagged Polκ was eluted with elution buffer (50 mM Tris pH 7.5, 300 mM NaCl, 2 mM $MgCl_2$, 1 mM DTT, 10% glycerol and 10 mM imidazole). Elution fractions containing the target proteins were pooled and dialyzed against dialysis buffer (50 mM Tris pH 7.5, 300 mM NaCl, 2 mM $MgCl_2$, 1 mM DTT and 10% glycerol) at 4 °C overnight. After dialysis, protein fractions were concentrated to 100 µl

using centrifugal filters with a molecular weight cutoff of 30,000 (Amicon) and subsequently aliquoted, flash-frozen in liquid nitrogen and stored at −80 °C.

Primer A: 5′-ATGCGGATCCAATGGATAACAAGCAAGAAGCAGAG-3′
Primer B: 5′-ATGCCTCGAGCTACTTGAAGAATCTGTCGATGGTG-3′
Primer C: 5′-ATGCGGATCCAAAACATCACCAGAAGAGCATTA CTAG-3′

Plasmids for expressing *X. laevis* WT and CD Polκ in rabbit reticulocytes were kind gifts from J. Gautier[36]. Briefly, 2 µg of pCMV-Sport-Polκ was incubated with 100 µl of TnT Sp6 Quick master mix (Promega) supplemented with 4 µl of 1 mM methionine for 90 min at 30 °C. The reaction volume was subsequently adjusted to 400 µl with PBS and DNA was precipitated by the addition of 0.06% polymin-P and incubation for 30 min at 4 °C with rotation. The mixture was then centrifuged at 14,000*g* for 30 min and the proteins in the supernatant were precipitated with saturated ammonium sulfate to a final concentration of 55% for 30 min at 4 °C with rotation, followed by centrifugation at 16,000*g* for 30 min. The protein pellet was subsequently resuspended in 15 µl of ELB, dialyzed for 3 h at 4 °C in ELB. As a negative control, a reaction without DNA was performed. The Polκ protein preparations obtained using this method were used for gap-filling synthesis experiments (Extended Data Fig. 1d).

Plasmid pulldown

Plasmid pulldowns were performed as described previously[22]. Briefly, 6 µl of streptavidin-coupled magnetic beads (Dynabead M-280, Invitrogen) per pulldown reaction were equilibrated with wash buffer 1 (50 mM Tris-HCl pH 7.5, 150 mM NaCl, 1 mM EDTA pH 8 and 0.02% Tween-20) and then incubated with 12 pmol of biotinylated LacI at RT for 40 min. The beads were washed four times with pulldown buffer 1 (10 mM HEPES pH 7.7, 50 mM KCl, 2.5 mM $MgCl_2$, 250 mM sucrose, 0.25 mg ml^{-1} BSA and 0.02% Tween-20), resuspended in 40 µl and stored on ice until used. At the indicated time points, 10 µl of reaction was added to the beads and rotated for 30 min at 4 °C. The beads were subsequently washed twice in wash buffer 2 (10 mM HEPES pH 7.7, 50 mM KCl, 2.5 mM $MgCl_2$, 0.25 mg ml^{-1} BSA and 0.03% Tween-20) and resuspended in 40 µl of 2× Laemmli sample buffer.

Chromatin spin down

Demembranated *Xenopus* sperm chromatin was prepared as described previously[86] and stored at −80 °C at a concentration of 100,000 sperm chromatin per µl (320 ng $µl^{-1}$). For analysis of UV-damaged chromatin, sperm chromatin was diluted to 25,000 sperm chromatin per µl in ELB, deposited on parafilm and irradiated with 2,000 J m^{-2} (for nonreplicating reactions) or 20 J m^{-2} (for replicating reactions) of UV-C. For nonreplicating reactions, HSS and NPE were premixed at a 1:2 ratio to block licensing. Subsequently, undamaged or UV-damaged sperm chromatin was added at a final concentration of 16 ng $µl^{-1}$. For replicating reactions, sperm chromatin was licensed in one volume of HSS for 30 min followed by the addition of two volumes of NPE. At the indicated time points, 8 µl of replication reaction was stopped with 60 µl of ELB supplemented with 0.2% Triton-X. The mixture was carefully layered on top of a sucrose cushion (10 mM HEPES pH 7.7, 50 mM KCl, 2.5 mM $MgCl_2$ and 500 mM sucrose) and spun for 1 min at 6,800*g* in a swing-bucket centrifuge at 4 °C. The chromatin pellet was carefully washed twice with 200 µl of ice-cold ELB and resuspended in 2× Laemmli buffer.

AlphaFold model generation

Molecular models were predicted using AlphaPulldown 0.30.0 (ref. 77), running AlphaFold 2.3.1 (ref. 78). AlphaPulldown parameters were as follows: cycles = 3, models = 5 and predictions per model = 1. Structure predictions were generated for *X. laevis* Q6DFE4 (POLK), P18248 (PCNA), Q6NRK6 (REV1), D0VEW8 (REV3), Q8QFR4 (REV7), O93610 (POLD2), Q76LD3 (POLD3) and P62972 (UBIQP), individually and as complexes of either full-length proteins or protein fragments.

Models were evaluated on their predicted local distance difference test[78], interface predicted template modeling[77,87], predicted template modeling[78] and predicted aligned error[88] scores. From each prediction, the best model as determined by AlphaPulldown was selected for inclusion in the final complex models.

Model building was performed using UCSF ChimeraX[89,90]. The catalytic complex was modeled on a scaffold of human Polκ holoenzyme with Ub-PCNA (Protein Data Bank (PDB) 7NV1 (ref. 55)).

The noncatalytic complex was modeled on a scaffold of the yeast Polζ (PDB 6V93 (ref. 69)). To establish the relative position of Polζ to PCNA, a structure of processive human Polδ holoenzyme was used (PDB 6TNY (ref. 91)). The monoubiquitinated PCNA and scaffold DNA attached to the polymerase complex was modeled on a structure of monoubiquitinated PCNA (PDB 3TBL (ref. 80)).

CHROMASS

CHROMASS experiments were performed as previously described[62]. Briefly, isolated sperm chromatin was either untreated or treated with 2,000 J m^{-2} of UV-C. Each reaction was performed in quadruplicate. The sperm chromatin was then incubated at a final concentration of 16 ng $µl^{-1}$ in nonlicensing extracts that were mock-treated, Polκ-depleted or Rev1-depleted. Reactions were stopped after 45 min. Specifically, 10 µl of replication reaction was stopped with 60 µl of ELB supplemented with 0.2% Triton-X and chromatin spin down performed as described above. The chromatin pellet was then resuspended in 100 µl of denaturation buffer (9 M urea and 100 mM Tris-HCl pH 8) and transferred to a new low-binding tube. Cysteines were reduced (1 mM DTT for 15 min at RT) and alkylated (0.55 M chloroacetamide for 40 min at RT protected from light). Proteins were first digested with 0.5 µg of LysC (2.5 h at RT) and then with 0.5 µg of trypsin at 30 °C overnight. Peptides were acidified with 10% trifluoroacetic acid (pH < 4), followed by the addition of 400 mM NaCl, and purified by StageTip (C18 material). For this, StageTips were first activated in 100% methanol, then equilibrated in 80% acetonitrile in 0.1% formic acid and finally washed twice in 0.1% formic acid. Samples were loaded onto the equilibrated stage tips and washed twice with 50 µl of 0.1% formic acid. StageTip elution was performed with 80 µl of 25% acetonitrile in 0.1% formic acid; eluted samples were dried to completion in a SpeedVac at 60 °C, dissolved in 10 µL 0.1% formic acid and stored at −20 °C until MS analysis.

MS data acquisition

All MS samples were analyzed on an EASY-nLC 1200 system (Thermo) coupled to an Orbitrap Exploris 480 MS instrument (Thermo). Of the $n = 4$ biochemical replicates, 50% were analyzed per run (R1–R4). Afterward, an additional $n = 4$ technical replicates were performed by mixing 25%:25% of R1:R2 (R5), R2:R3 (R6), R3:R4 (R7) and R4:R1 (R8), totaling $n = 8$ technical replicates. Separation of peptides was performed using 20-cm columns (75-µm internal diameter) packed in house with ReproSil-Pur 120 C18-AQ 1.9-µm beads (Dr. Maisch). Elution of peptides from the column was achieved using a gradient ranging from buffer A (0.1% formic acid) to buffer B (80% acetonitrile in 0.1% formic acid), at a flow of 250 nl min^{-1}. The gradient length was 80 min per sample, including ramp up and wash out, with an analytical gradient of 58 min ranging from 7% B to 34% B. Analytical columns were heated to 40 °C using a column oven and ionization was achieved using a NanoSpray Flex NG ion source. Spray voltage was set to 2 kV, ion transfer tube temperature was set to 275 °C and RF funnel level was set to 40%. The full scan range was set to 300–1,300 m/z, MS1 resolution was set to 120,000, MS1 automated gain control (AGC) target was set to '200' (2,000,000 charges) and MS1 maximum injection time was set to 'auto'. Precursors with charges 2–6 were selected for fragmentation using an isolation width of 1.3 m/z and fragmented using higher-energy collision disassociation with a normalized collision

energy of 25. Precursors were excluded from resequencing by setting a dynamic exclusion of 80 s. The MS2 AGC target was set to '200' (200,000 charges), intensity threshold was set to 360,000 charges per second, MS2 maximum injection time was set to 'auto', MS2 resolution was set to 30,000 and number of dependent scans was set to 13.

MS data analysis

All MS RAW data were analyzed using the freely available MaxQuant software (version 1.5.3.30)[92] in a single computational run. Default MaxQuant settings were used, with exceptions specified below. For the generation of theoretical spectral libraries, the *X. laevis* FASTA database was downloaded from UniProt on October, 3 2022. In silico digestion of proteins to generate theoretical peptides was performed with trypsin, allowing up to three missed cleavages. The minimum peptide length was set to six and maximum peptide mass was set to 6,000 Da. Allowed variable modifications were oxidation of methionine (default), protein N-terminal acetylation (default), deamidation of asparagine and glutamine, peptide N-terminal glutamine to pyroglutamate conversion, dioxidation of tryptophan and replacement of three protons by iron (cation Fe(III)) on aspartate and glutamate. These variable modifications were determined by an initial analysis of the RAW data using pFind version 3.1.6 in 'open search' mode[89] to unbiasedly determine any known modifications (from the Unimod database) affecting >0.5% of peptide–spectrum matches (PSMs) across all samples. The maximum number of variable modifications per peptide was set to three. Label-free quantification (LFQ) using MaxLFQ was enabled[93] with 'fast LFQ' disabled. Matching between runs was enabled, with an alignment window of 20 min and a match time window of 1 min. A stringent MaxQuant 1% false discovery rate (FDR) control was applied at the PSM, protein and site-decoy levels (default).

MS data annotation and quantification

The *X. laevis* FASTA databases downloaded from UniProt lacked comprehensive gene name annotations. Missing or uninformative gene names were, when possible, semiautomatically curated, as described previously[15]. Quantification of the MaxQuant output files ('proteinGroups.txt') and all statistical handling were performed using Perseus software (version 1.5.5.3)[94]. In total, $n = 8$ technical replicates (derived from $n = 4$ biochemical replicates) were analyzed. For quantification purposes, all LFQ-normalized protein intensity values were $\log_2$-transformed and filtered for presence in eight of eight replicates in at least one experimental condition. Missing values were inputted below the global experimental detection limit at a downshift of 1.8 and a randomized width of 0.15 (in $\log_2$ space). The statistical significance of differences was in all cases tested using two-tailed Student's two-sample *t*-testing, with permutation-based FDR control applied to ensure a corrected *P* value (that is, *q* value) of <1%. Proteins not enriched over the no-DNA control in at least one CHROMASS condition (FDR < 1%, $s_0 = 1$ and 2,500 rounds of randomization) were removed from the analysis, after which previously inputted values were reinputted on the basis of the new total matrix. Final biological differences were determined using two-tailed Student's two-sample *t*-testing (FDR < 1%, $s_0 = 0.5$ and 2,500 rounds of randomization) on the remaining CHROMASS-enriched proteins.

Cell culture

Cells were cultured in high-glucose DMEM with glutaMAX Supplement and pyruvate (Gibco) supplemented with 10% FBS (Gibco) and 100 U per ml of penicillin–streptomycin (Gibco) at 37 °C with 5% CO_2.

Generation of U2OS Flp-In T-REx *POLK*-KO cells

U2OS Flp-In T-REx cells were a kind gift from H. Piwnica-Worms. Four different gRNAs targeting different regions of *POLK* (5′-TAGGTTCAACACACCTGACG-3′, 5′-ATACATATAGATACCTCGTC-3′, 5′-ATACCGAGCTGTGAGTAAAG-3′ and 5′-AGGACAGGAAACACCAACAA-3′) were cloned into pSpCas9(BB)-2A-Puro (PX459) V2.0 (Addgene, 62988). sgRNA-containing plasmids were transfected into U2OS Flp-In T-REx cells using Dharmacon 1 (Horizon Discovert T-2005-01) transfection reagent according to the manufacturer's protocol. After 24 h of incubation, transfected cells were selected with 1 µM puromycin for 48 h and plated sparsely to isolate single colonies. Single colonies were screened by qPCR for a lack of *POLK* mRNA using a primer pair (forward, 5′-TTGGGTCTAGGTTCAACACACC-3′; reverse, 5′-GCAAGCTCACTGCAAAGTTCT-3′). To perform the qPCR, total RNA was extracted using Qiagen RNeasy Mini (Qiagen 74104) according to the manufacturer's instructions. Complementary DNA (cDNA) was synthesized from total RNA using the iScript cDNA synthesis kit (Bio-Rad, 1708890) according to the manufacturer's instructions. qPCR was performed in 96-well plates using the mentioned primers and Brilliant III ultrafast SYBR green qPCR master mix (Agilent, 600882) in a Stratagene Mx3005P machine using standard thermocycling conditions.

Cloning of pcDNA5/FRT/TO/Venus–*POLK* constructs

Human WT and CD *POLK* (harboring D198A and E199A substitutions) cDNA sequences were a kind gift from O. Scharer. BamHI and NotI restriction sites were added using PCR (forward primer, 5′-ATGCGGATCCATG GATAGCACAAAGGAGAAGTGTGAC-3′; reverse primer, 5′-TATAGCGGCCGCTTACTTAAAAAATATATCAAGGGTATGTTTGGG-3′) and cloned into pcDNA5/FRT/TO-Venus. Constructs were sequence-verified.

Generation of *POLK*-KO cells stably expressing Venus–Polκ

To generate stable cell lines in the Flp-In system, U2OS Flp-In T-REx *POLK*-KO cells were cotransfected with the Flp recombinase-encoding plasmid pOG44 (Invitrogen) and a pcDNA5/FRT/TO plasmid encoding Venus–WT Polκ or Venus–CD Polκ at a 10:1 ratio using the jetOPTIMUS transfection reagent (Polyplus). Then, 48 h after transfection, cells were selected in medium supplemented with 5 µg ml^{-1} blasticidin S HCl and 200 µg ml^{-1} hygromycin B (Gibco) for 2–3 weeks. Expression from the Tet-ON inducible promoter in U2OS Flp-In T-REx cells was induced with 20 ng ml^{-1} doxycycline.

Colony formation assays

The cells were trypsinized, resuspended in medium and counted. A total of 200 cells were seeded per well in six-well plates with three wells per condition. Venus–Polκ-expressing Flp-In T-REx cells were induced with 20 ng ml^{-1} doxycycline. Then, 24 h after seeding, cells were treated with the indicated compound (31.25 pg ml^{-1} illudin S or 1 µM cisplatin) or left untreated. After seven additional days of growth, formed colonies were fixed and stained in a methyl violet solution (0.5% methyl violet and 25% methanol) and the number of colonies was quantified on a GelCount (Oxford Optronix). The survival after treatment with a given compound was calculated as the average number of colonies after treatment divided by the average number of colonies in the untreated condition multiplied by 100%. The experiments were performed three times independently and analyzed in PRISM (GraphPad). One-way analyses of variance (ANOVAs) with Tukey's multiple-comparisons tests were performed to test for statistical significance.

Western blot analysis of cell lysates

Cells were harvested by trypsinization, lyzed on ice in radioimmunoprecipitation assay buffer (10 mM Tris pH 7.4, 150 mM NaCl, 1 mM EDTA, 1% NP-40, 0.5% sodium deoxycholate and 0.1% SDS) supplemented with 1 mM DTT and cOmplete protease inhibitor cocktail (Roche) and sonicated with Bioruptor Plus (Diagenode). The lysate was cleared by centrifugation at 20,000*g* at 4 °C for 30 min and a BCA assay (Pierce) was used to measure protein concentrations. Samples were analyzed by SDS–PAGE and western blotting using anti-Polκ (Bethyl laboratories, A301-975A) and anti-tubulin (Abcam, ab6160) antibodies.

Base-editor tiling screen and analysis

An sgRNA library targeting the coding sequence of Polκ was designed. The gRNA oligonucleotide pool was synthesized by GenScript as an 83-nt oligonucleotide sequence, following a previously published design[48]. The oligonucleotide sequence consisted of primer sites for amplification with overhang sequences with Esp3I recognition sites and the gRNA: 5′-[forward primer (20 nt)]CGTCTCACACCG[sgRNA (20 nt)] GTTTCGAGACG[reverse primer (20 nt)]. The gRNA oligonucleotide pool was amplified using NEBNext Ultra II Q5 master mix (New England BioLabs) and the primers (forward, 5′-GTGTAACCCGTAGGGCACCT-3′; reverse, 5′-GTCGAGAGCAGTCCTTCGAC-3′). Amplicons were cloned into the Abe8e-Cas9-SpG lentiviral vector pRDA_479 (ref. 48) using Golden Gate cloning with Esp3I and T7 ligase. pRDA_479 was a gift from J. Doench and D. Root (Addgene, plasmid 179099). The ligated plasmid library was purified by PCR (NucleoSpin gel and PCR Clean-Up, Macherey-Nagel) and isopropanol precipitation and electroporated into Endura electrocompetent cells (Lucigen), which were grown at 30 °C for 16 h on agar with 100 µg ml^{-1} carbenicillin. Plasmid DNA was prepared from the colonies on the plates (NucleoBond Xtra Maxi, Macherey-Nagel). To confirm library representation, the gRNA inserts were amplified from the plasmid library using NEBNext Ultra II Q5 master mix and the primers D506_F and D702_R_PAGE_BE (Supplementary Table 3). Gel-purified amplicons were sequenced on a NextSeq2000 (Illumina). The Polκ tiling library was part of a larger adenosine base editing (ABE) and cytosine base editing (CBE) tiling library, for which only Polκ with ABE is analyzed here. Note that some CBE guides also score, most likely because of low-frequency editing beyond the optimal 4–8-nt editing window. A lentiviral library was produced by cotransfection of HEK293T/17 cells (American Type Culture Collection, CRL-11268) with the sgRNA plasmid library and lentiviral packaging plasmids pMD2.G and psPAX2 using Lipofectamine 3000 (Invitrogen) in Opti-MEM medium (Gibco). pMD2.G (Addgene, plasmid 12259) and psPAX2 (Addgene, plasmid 12260) were gifts from D. Trono. Then, 6 h after transfection, the medium was exchanged for DMEM GlutaMax supplemented with 10% FBS, 100 U per ml of penicillin–streptomycin and 1% BSA. Next, 48 h after transfection, the lentiviral supernatant was collected and filtered through a 0.45-µm syringe filter before storing at −80 °C. RPE1-hTERT *p53*$^{-/-}$ cells (a kind gift from D. Durocher) were cultured in DMEM GlutaMax supplemented with 10% FBS and 100 U per ml of penicillin–streptomycin and passaged every 3 days. The screen was performed as a duplicate (two separate transductions) at a coverage of >500-fold sgRNA representation, which was maintained throughout the screen. Cells were transduced with the lentiviral library at a low multiplicity of infection (0.3–0.4) and transductions were caried out by treating cells with 8 µg ml^{-1} polybrene and lentiviral supernatant for 24 h. Transduced cells were selected by treatment with 20 µg ml^{-1} puromycin for 24 h followed by trypsinization and reseeding in the same plates with 20 µg ml^{-1} puromycin for another 24 h. After selection, cells were passaged for 6 days before splitting into untreated or illudin-S-treated fractions, where they were passaged for an additional 12 days in medium with or without a low dose of illudin S (1.4 ng ml^{-1}). The dose of illudin S corresponds to a 20% reduction in cell numbers (LD_{20}) compared to the untreated condition in uninfected cells, which was determined in a titration experiment. Genomic DNA was extracted from cell pellets harvested after selection, which we consider the start of the screen (t_0) and at the final time point (t_{18}). The genomic DNA region containing the integrated sgRNA was amplified by PCR using NEBNext Ultra II Q5 master mix with the LCV2_forward and LCV2_reverse primers (Supplementary Table 3). A second PCR reaction introduced i5 and i7 multiplexing barcodes (Supplementary Table 3) and gel-purified PCR products were sequenced on Illumina NextSeq2000. Sequencing data of t_0, untreated t_{18} and illudin-S-treated t_{18} samples were converted to gRNA sequencing counts by MAGeCK[95] and mapping was performed to gRNAs tiling *POLK* and control gRNAs (essential splice sites, nontargeting and intergenic)[48]. Low-abundance gRNAs were removed (counts < 30) and raw sequencing counts were normalized per condition replicate to $\log_2$ transcripts per million ($\log_2$TPM). The $\log_2$TPM values were compared using limma[96] for three sample pairs (t_0 versus untreated t_{18}, t_0 versus illudin-S-treated t_{18} and untreated t_{18} versus illudin-S-treated t_{18}) and the fold change, *P* value and *q* value were collected for each gRNA. gRNA editing outcomes were predicted on the basis of the editing of all adenines within the editing window of positions 4–8 (ref. 97).

Reproducibility

A minimum of two independent experiments were conducted for each experimental result shown in this manuscript.

Reporting summary

Further information on research design is available in the Nature Portfolio Reporting Summary linked to this article.

Data availability

The MS proteomics data were deposited to the ProteomeXchange Consortium through the PRIDE[98] partner repository with the dataset identifier PXD044258. Source data are provided with this paper.

References

81. Lebofsky, R., Takahashi, T. & Walter, J. C. DNA replication in nucleus-free *Xenopus* egg extracts. *Methods Mol. Biol.* **521**, 229–252 (2009).
82. Sparks, J. L. et al. The CMG helicase bypasses DNA–protein cross-links to facilitate their repair. *Cell* **176**, 167–181 (2019).
83. Sobeck, A. et al. Fanconi anemia proteins are required to prevent accumulation of replication-associated DNA double-strand breaks. *Mol. Cell. Biol.* **26**, 425–437 (2006).
84. Knipscheer, P. et al. The Fanconi anemia pathway promotes replication-dependent DNA interstrand cross-link repair. *Science* **326**, 1698–1701 (2009).
85. Räschle, M. et al. Mechanism of replication-coupled DNA interstrand crosslink repair. *Cell* **134**, 969–980 (2008).
86. Sparks, J. & Walter, J. C. Extracts for analysis of DNA replication in a nucleus-free system. *Cold Spring Harb. Protoc.* **2019**, prot097154 (2019).
87. Evans, R. et al. Protein complex prediction with AlphaFold-Multimer. Preprint at *bioRxiv* https://doi.org/10.1101/2021.10.04.463034 (2022).
88. Varadi, M. et al. AlphaFold Protein Structure Database: massively expanding the structural coverage of protein-sequence space with high-accuracy models. *Nucleic Acids Res.* **50**, D439–D444 (2022).
89. Goddard, T. D. et al. UCSF ChimeraX: meeting modern challenges in visualization and analysis. *Protein Sci.* **27**, 14–25 (2018).
90. Pettersen, E. F. et al. UCSF ChimeraX: structure visualization for researchers, educators, and developers. *Protein Sci.* **30**, 70–82 (2021).
91. Lancey, C. et al. Structure of the processive human Pol δ holoenzyme. *Nat. Commun.* **11**, 1109 (2020).
92. Cox, J. & Mann, M. MaxQuant enables high peptide identification rates, individualized p.p.b.-range mass accuracies and proteome-wide protein quantification. *Nat. Biotechnol.* **26**, 1367–1372 (2008).
93. Cox, J. et al. Accurate proteome-wide label-free quantification by delayed normalization and maximal peptide ratio extraction, termed MaxLFQ. *Mol. Cell. Proteomics* **13**, 2513–2526 (2014).
94. Tyanova, S. et al. The Perseus computational platform for comprehensive analysis of (prote)omics data. *Nat. Methods* **13**, 731–740 (2016).
95. Li, W. et al. MAGeCK enables robust identification of essential genes from genome-scale CRISPR/Cas9 knockout screens. *Genome Biol.* **15**, 554 (2014).

96. Ritchie, M. E. et al. limma powers differential expression analyses for RNA-sequencing and microarray studies. *Nucleic Acids Res.* **43**, e47 (2015).
97. Richter, M. F. et al. Phage-assisted evolution of an adenine base editor with improved Cas domain compatibility and activity. *Nat. Biotechnol.* **38**, 883–891 (2020).
98. Perez-Riverol, Y. et al. The PRIDE database resources in 2022: a hub for mass spectrometry-based proteomics evidences. *Nucleic Acids Res.* **50**, D543–D552 (2022).

Acknowledgements

We thank J. Gautier (Columbia University) for sharing Polκ-expressing constructs, D. Durocher (University of Toronto) for the RPE1-hTERT *p53*$^{-/-}$ cells and staff of the CPR/ReNew Genomics Platform for support: H. Wollmann, M. Michaut and A. Kalvisa. We also thank members of the Duxin laboratory and J. Walter for feedback on the manuscript. The Novo Nordisk Foundation Center for Protein Research is supported financially by the Novo Nordisk Foundation (grant agreement NNF14CC0001). This project has received funding from the European Research Council under the European Union's Horizon 2020 research and innovation program (grant agreement 715975) and from the Novo Nordisk Foundation (grant NNF22OC0074140). B.B. is supported by the European Molecular Biology Organization (grant agreement no. ALTF 1149-2020). Work in J.N.'s lab was supported by a Novo Nordisk Fonden distinguished investigator grant (NNF23OC0082227) and a grant from the Danish Cancer Society (R269-A15586-B71). T.C.R.M. was supported by a Novo Nordisk Fonden Hallas-Møller emerging investigator grant (NNF22OC0073571), the Danish National Research Foundation (DNRF115) and the Carlsberg Foundation (CF21-0571). J.P.D. is part of the European doctoral network (Replifate, grant agreement #101072903). We also extend our gratitude to J. Lukas for his exceptional leadership, which has elevated the Center for Protein Research to the forefront of biological research.

Author contributions

S.S.B. performed all experiments unless stated otherwise. A.C. generated the AlphaFold models in Figs. 1c and 7e,f and Extended Data Figs. 1b,c and 7c under the supervision of T.M. S.M.A. and B.M. performed the CRISPR base-editor tiling screen (Fig. 1b and Extended Data Fig. 1a) under the supervision of J.N. E.P.T.H. provided technical advice on the base-editor screen. N.D. designed the CRISPR library and performed statistical analysis of the sequencing data. I.A.H. performed MS analysis on CHROMASS samples (Fig. 6 and Extended Data Fig. 6) under the supervision of M.L.N. L.S and B.B. generated the p3d-Phen-A minor groove DNA substrate under the supervision of S.S. and J.P.D. I.G. performed the experiment in Fig. 6d and preliminary experiments for this project. D.S. provided the AP-ICL-containing plasmid. S.A.G. generated the *POLK*-KO cells. S.M.A. performed the colony assay experiments (Fig. 7a–d). A.Z. assisted with recombinant Polκ protein purification. S.S.B. and J.P.D. designed and analyzed the experiments. S.S.B. and J.P.D. prepared the manuscript with feedback and input from all authors of the manuscript.

Competing interests

The authors declare no competing interests.

Additional information

Extended data is available for this paper at https://doi.org/10.1038/s41594-024-01395-3.

Supplementary information The online version contains supplementary material available at https://doi.org/10.1038/s41594-024-01395-3.

Correspondence and requests for materials should be addressed to Julien P. Duxin.

Peer review information *Nature Structural & Molecular Biology* thanks Vincent Pagès and the other, anonymous, reviewer(s) for their contribution to the peer review of this work. Peer reviewer reports are available. Primary Handling Editor: Dimitris Typas, in collaboration with the *Nature Structural & Molecular Biology* team.

https://doi.org/10.1038/s41594-024-01395-3

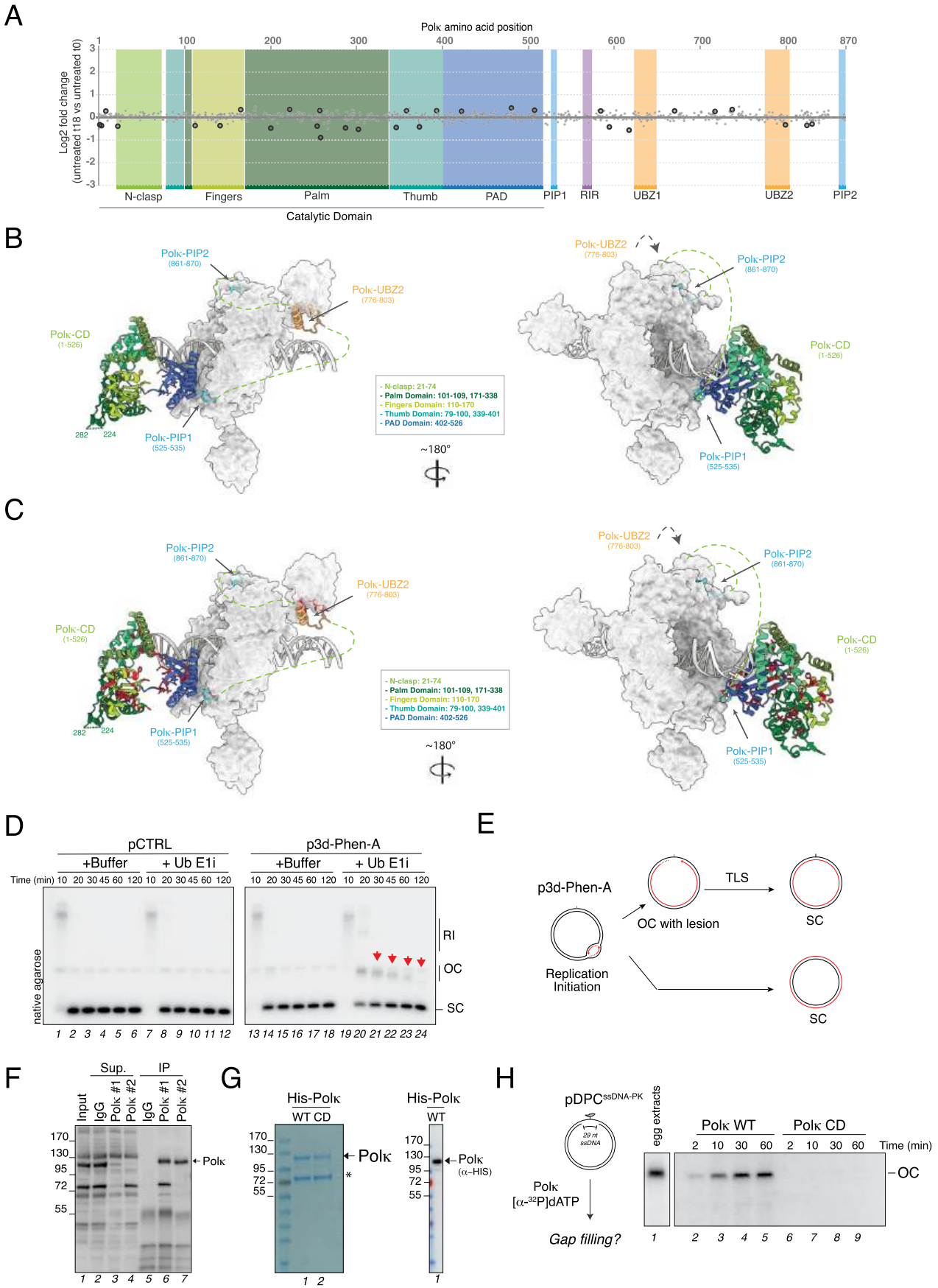

Extended Data Fig. 1 | See next page for caption.

https://doi.org/10.1038/s41594-024-01395-3

Extended Data Fig. 1 | a) Dot plot showing the results of the Polκ CRISPR base editor tiling screen comparing t0 and t18 of the untreated condition. Each guide is shown as a dot. X-axis represents amino acid position in Polκ. Y-axis represents Log2 fold changes between t18 and t0 of the untreated condition. Larger dots represent guides which are significantly changing between the two conditions (p-value ≤ 0.01). The various domains of Polκ are indicated. The significance and fold change was derived from limma (see Methods) **b**) Composite molecular model of human Polκ. Dashed lines represent disordered regions that are not present in the model. The model was generated as described in Fig. 1c. **c**) Composite molecular model of human Polκ with point mutations derived from the base editor tiling screen. Dashed lines represent disordered regions that are not present in the model. Point mutations are highlighted in red. The left panel is a duplicate of Fig. 1c. **d**) pCTRL and p3d-Phen-A were replicated in the presence or absence of ubiquitin E1 inhibitor. Reaction samples were analyzed as in Fig. 1h. **e**) Schematic diagram illustrating the replication intermediates generated during the replication of p3d-Phen-A. **f)** Western blot of the immunoprecipitation of Polκ using our generated *Xenopus* Polκ antibody. Sup., supernatant; IP, immunoprecipitation. Polκ #1 and Polκ #2 denotes two different affinity purifications generated from the same rabbits. **g)** Coomassie blue staining of recombinant Polκ WT and Polκ CD purified from *E.coli*. * denotes a contaminant not recognized by the anti-HIS antibody (right immunoblot). **h**) Schematic representation of gap filling synthesis (left scheme) when $pDPC^{ssDNA}$ is incubated with Polκ WT, Polκ CD, or whole egg cytosolic egg extract (HSS) in the presence of [α-^{32}P]dATP. Note the absence of DNA synthesis in the Polκ CD reaction (lanes 6-9).

https://doi.org/10.1038/s41594-024-01395-3

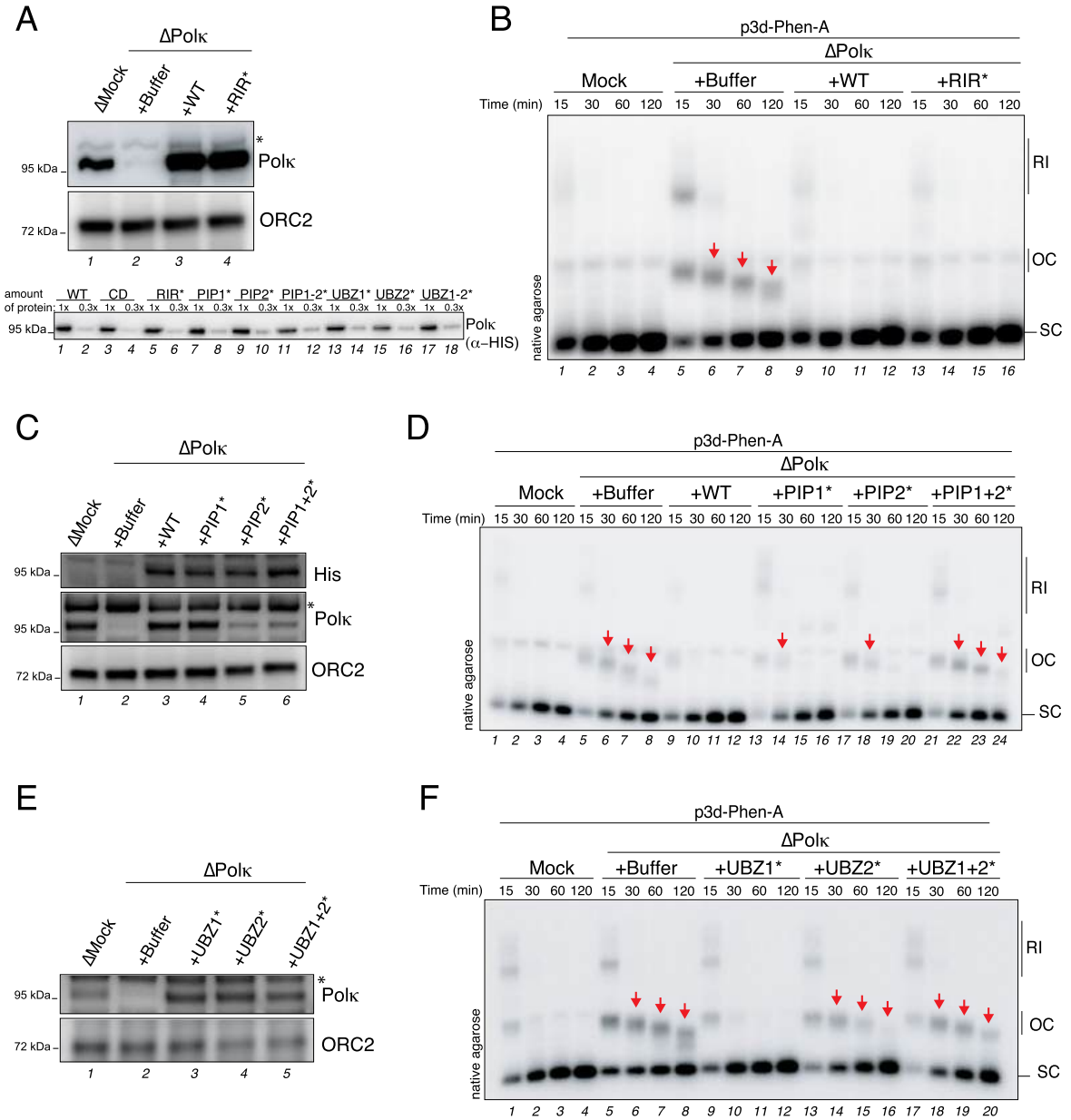

Extended Data Fig. 2 | a) Polκ-depleted extracts were supplemented with either buffer (+Buffer), wild-type Polκ (+WT), or RIR (RIR*) Polκ mutant. Samples were blotted with the indicated antibodies (top immunoblots). To ensure that the same amount of protein was added back to the extracts, the different Polκ preparations used in this study were titrated, and equal amounts were confirmed via immunoblotting (via HIS antibody, bottom immunoblot). 1x corresponds to the amount needed to add back roughly endogenous levels of Polκ (when added to 10% F.C in NPE). We unfortunately lack the Coomassie stain of various mutants. **b)** Extracts from (A) were used to replicate p3d-Phen-A. Samples were analyzed as in Fig. 1h. **c)** Polκ-depleted extracts were supplemented with either buffer (+Buffer), wild-type Polκ (+WT), PIP1 (PIP1*), PIP2 (PIP2*) or PIP1 and PIP2 (PIP1 + 2*) Polκ mutants. Samples were blotted with the indicated antibodies. Note that the Polκ antibody was generated against Polκ C-terminal end which encompasses PIP2. This antibody exhibits lower affinity for Polκ PIP2* compared to Polκ WT and Polκ PIP1*. The 6xHis tag of the recombinant protein is located on the N-terminal end. **d)** Extracts from (C) were used to replicate p3d-Phen-A. Samples were analyzed as in Fig. 1h. **e)** Polκ-depleted extracts were supplemented with either buffer (+Buffer), wild-type Polκ (+WT), UBZ (UBZ1*), UBZ (UBZ2*) or UBZ1 and UBZ2 (UBZ1 + 2*) Polκ mutants. Samples were blotted with the indicated antibodies. **f)** Extracts from (E) were used to replicate 3d-Phen-A. Samples were analyzed as in Fig. 1h.

https://doi.org/10.1038/s41594-024-01395-3

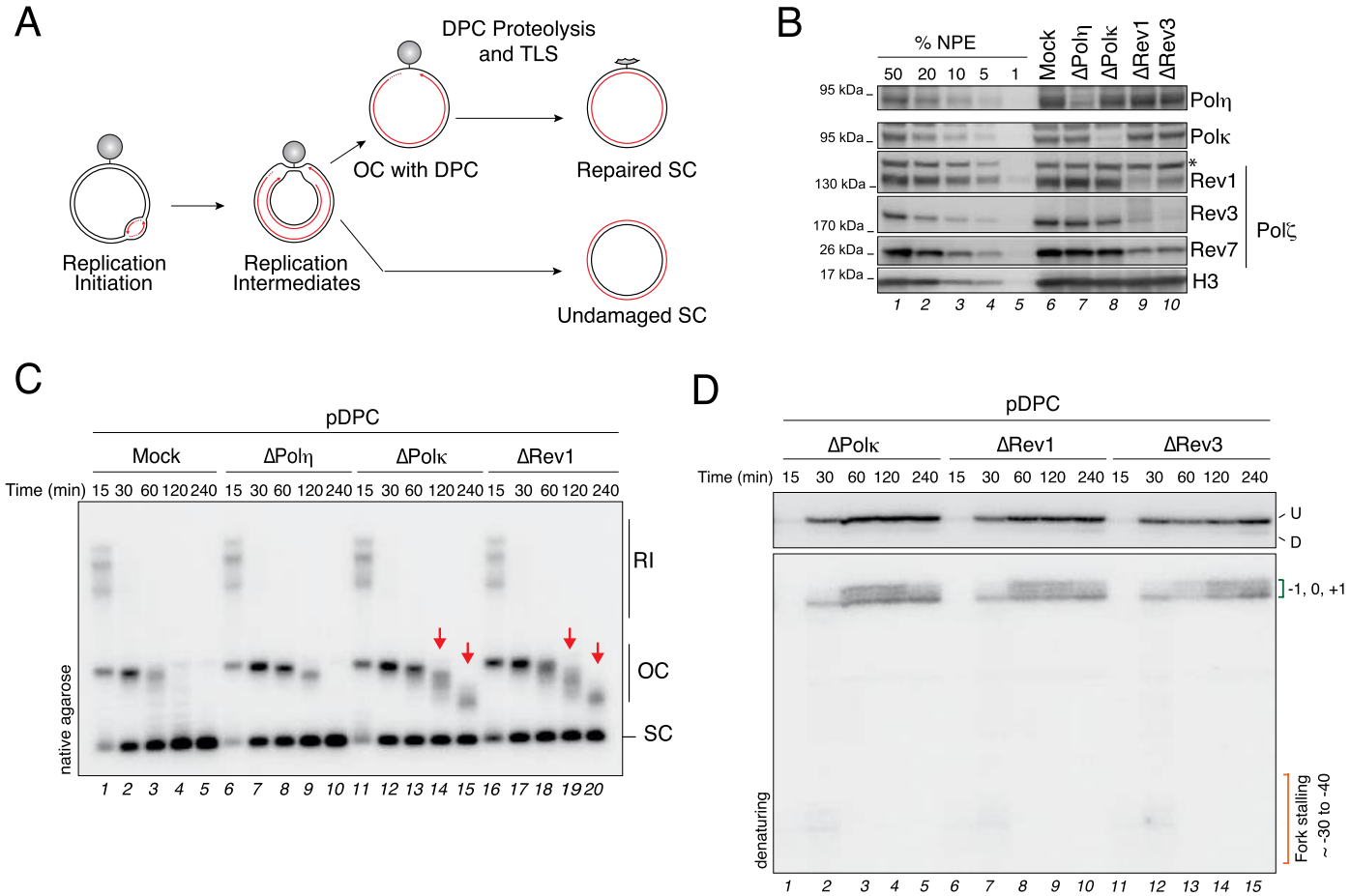

Extended Data Fig. 3 | a) Replication intermediates generated during replication of pDPC[57]. **b)** Mock-, Polη-, Polκ-, Rev1-, or Rev3-depleted extracts were blotted with the indicated antibodies. **c)** pDPC was replicated in egg extracts in mock-, Polη-, Polκ-, or Rev1-depleted extracts. Reaction samples were analyzed as in Fig. 1h. **d)** pDPC was replicated in Polκ- or Rev1-, or Rev3-depleted egg extracts. Samples were digested, separated on a denaturing polyacrylamide gel and analyzed as in Fig. 3c.

https://doi.org/10.1038/s41594-024-01395-3

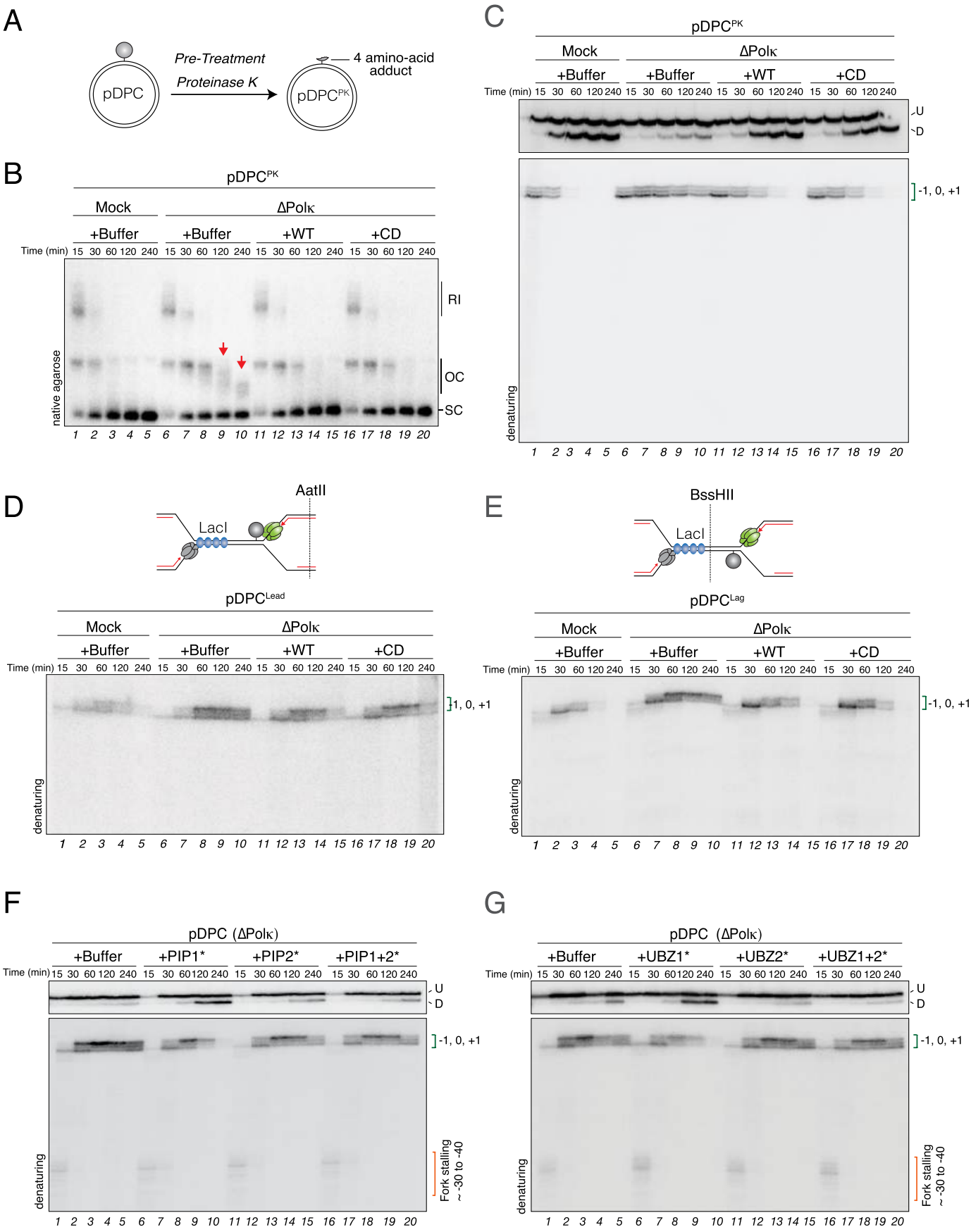

Extended Data Fig. 4 | See next page for caption.

https://doi.org/10.1038/s41594-024-01395-3

Extended Data Fig. 4 | a) Generation of pDPC^{PK}[56]. **b)** Mock- and Polκ-depleted egg extracts were used to replicate pDPC^{PK}. Polκ-depleted extracts were supplemented with either buffer (+Buffer), wild-type (+WT), or catalytically inactive (+CD) Polκ. Samples were analyzed as in Fig. 1h. **c)** Samples from (B) were digested and analyzed as in Fig. 3c. **d)** pDPC^{Lead} was replicated in either mock- or Polκ-depleted egg extracts in the presence of LacI[57]. Polκ-depleted extracts were supplemented with either buffer (+Buffer), wild-type Polκ (+WT), or catalytically inactive Polκ (+CD). Samples were digested with AatII, separated on a denaturing polyacrylamide gel and analyzed as in Fig. 3c. **e)** Extracts from (D) were used to replicate pDPC^{Lag}[57]. Samples were digested with BssHII, separated on a denaturing polyacrylamide gel and analyzed as in Fig. 3c. **f**) Polκ-depleted egg extracts were supplemented with either buffer (+Buffer), recombinant PIP1 (+PIP1*), PIP2 (+PIP2*) or PIP1 and PIP2 (PIP1 + 2*) Polκ mutants. Extracts were then used to replicate pDPC. Samples were digested and analyzed as in Fig. 3c. **g**) Polκ-depleted egg extracts were supplemented with either buffer (+Buffer), UBZ1(+UBZ1*), UBZ2 (+UBZ2*), or UBZ1 and UBZ2 (+UBZ1 + 2*) Polκ mutants. Extracts were then used to replicate pDPC. Samples were analyzed as in Fig. 3c.

https://doi.org/10.1038/s41594-024-01395-3

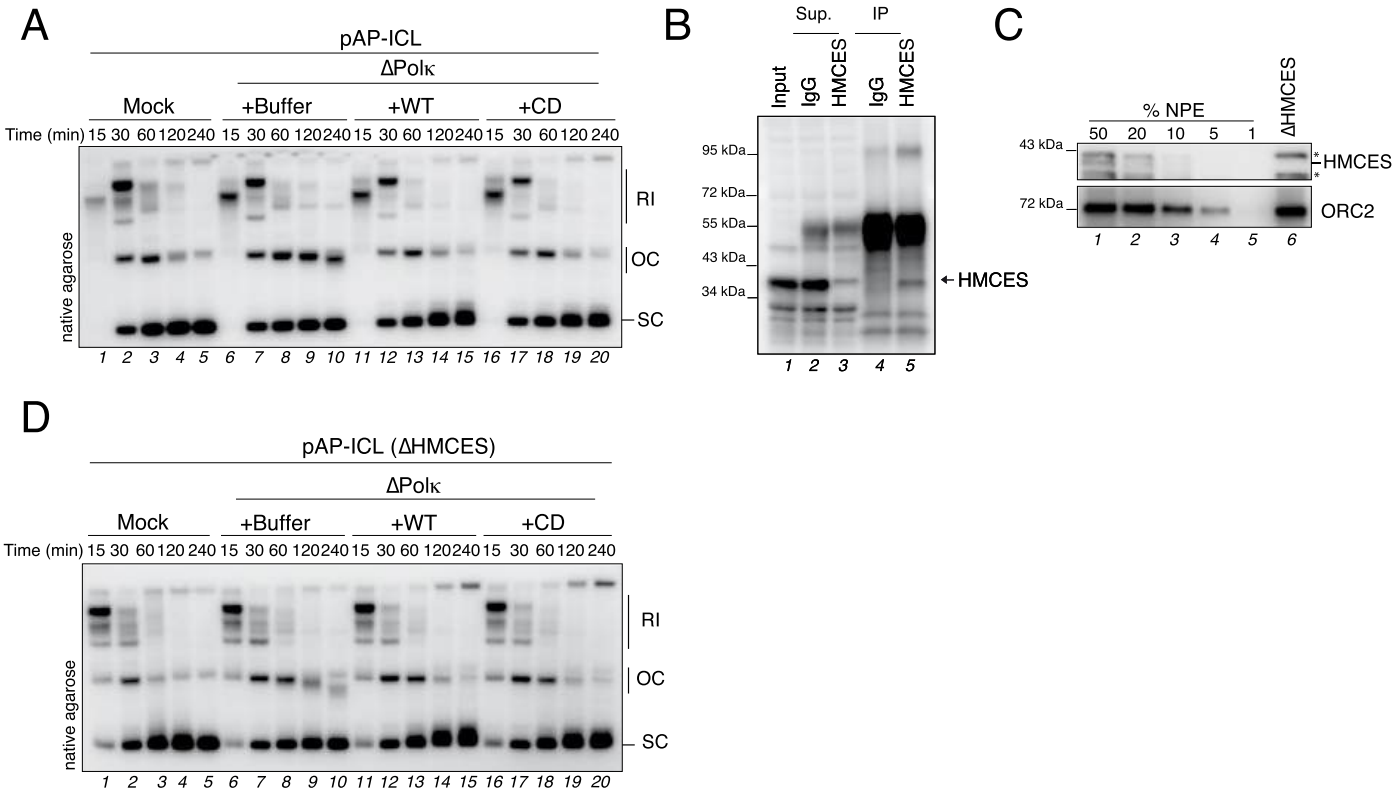

Extended Data Fig. 5 | a) Mock- and Polκ-depleted egg extracts were used to replicate pAP-ICL. Polκ-depleted extracts were supplemented with either buffer (+Buffer), wild-type Polκ (+WT), or catalytically inactive Polκ (+CD). The samples were analyzed as in Fig. 1h. **b)** Western blot of the immunoprecipitation of HMCES. Sup., supernatant; IP, immunoprecipitation. **c)** Mock- and HMCES-extracts were blotted with the indicated antibodies. * indicates a non-specific band. **d)** HMCES-depleted extracts were either mock- or Polκ-depleted and were subsequently used to replicate pAP-ICL. Polκ-depleted extracts were supplemented with either buffer (+Buffer), wild-type Polκ (+WT), or catalytically inactive Polκ (+CD). The samples were analyzed as in Fig. 1h.

https://doi.org/10.1038/s41594-024-01395-3

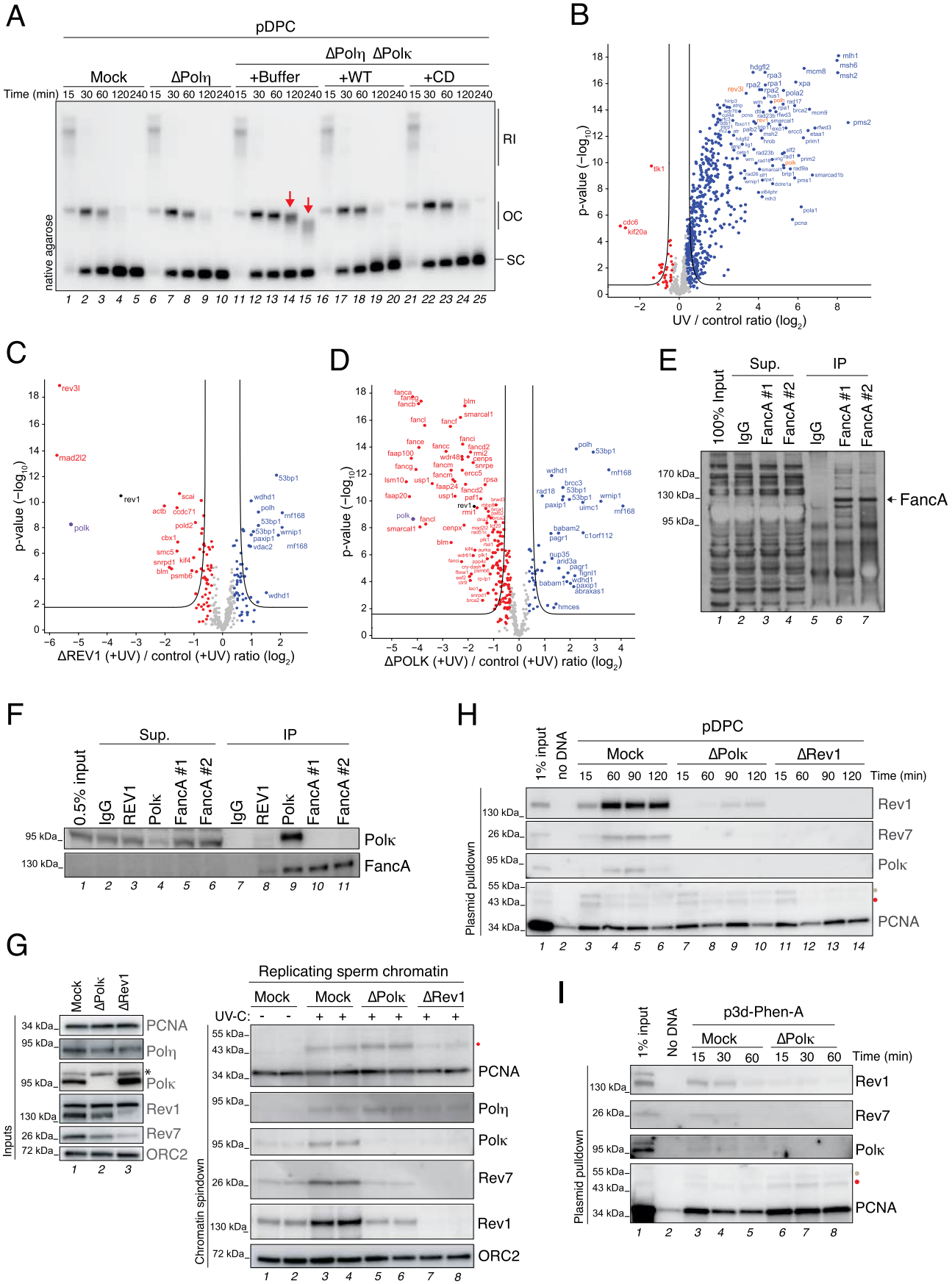

Extended Data Fig. 6 | See next page for caption.

https://doi.org/10.1038/s41594-024-01395-3

Extended Data Fig. 6 | a) Mock-, Polη-, or double Polη- and Polκ-depleted egg extracts were used to replicate pDPC. Polκ-depleted extracts were supplemented with either buffer (+Buffer), wild-type Polκ (+WT), or catalytically inactive Polκ (+CD). Samples were analyzed as in Fig. 1h. **b)** MS analysis of protein recruitment to UV-treated compared to untreated sperm chromatin. The volcano plot shows the difference in abundance of proteins between the two sample conditions (x-axis), plotted against the *p*-value resulting from two- tailed Student's two-sample t-testing (y-axis). Proteins significantly down- or up-regulated (FDR < 5%) upon UV treatment are represented in red or blue, respectively. TLS polymerases are highlighted in orange. n = 4 biochemical and n = 8 technical replicates, significance was determined via two-tailed Student's two-sample t-testing, with permutation-based FDR control (s0 = 0.5) to ensure an adjusted p-value (that is q-value) of <0.05 in all cases. The significance line is drawn at q = 0.01. **c)** Same experiment as in (B) but comparing mock- to Rev1-depleted extracts. Small red dots, 1% < FDR < 5%; large red dots, FDR < 1%. Polκ and Rev1 are highlighted in purple and black, respectively. **d)** Same experiment as in (B) but comparing mock- to Polκ-depleted extracts. Small red dots, 1% < FDR < 5%; large red dots, FDR < 1%. Polκ and Rev1 are highlighted in purple and black, respectively. **e**) Western blot of FancA immunoprecipiates. Sup., supernatant; IP, immunoprecipitation. FancA #1[83] and was used to validate that our FancA antibody (FancA #2) immunoprecipitates the same protein. **f)** Western blot of the co-immunoprecipitation of Polκ with FancA. Sup., supernatant; IP, immunoprecipitation. **g)** Sperm chromatin was either untreated or treated with 20 J/m2 of UV-C and then added to replicating mock-, Polκ- or Rev1-depleted extracts. Chromatin samples of duplicated reactions were isolated at 60 min, and the proteins associated were blotted with the indicated antibodies. **h)** pDPC was replicated in either mock, Polκ or Rev1-depleted extracts. Reactions were subjected to plasmid pull-down and samples were blotted with the indicated antibodies. **i)** p3d-Phen-A was replicated in either mock or Polκ-depleted extracts. Reactions were subjected to plasmid pull-down and samples were blotted with the indicated antibodies.

https://doi.org/10.1038/s41594-024-01395-3

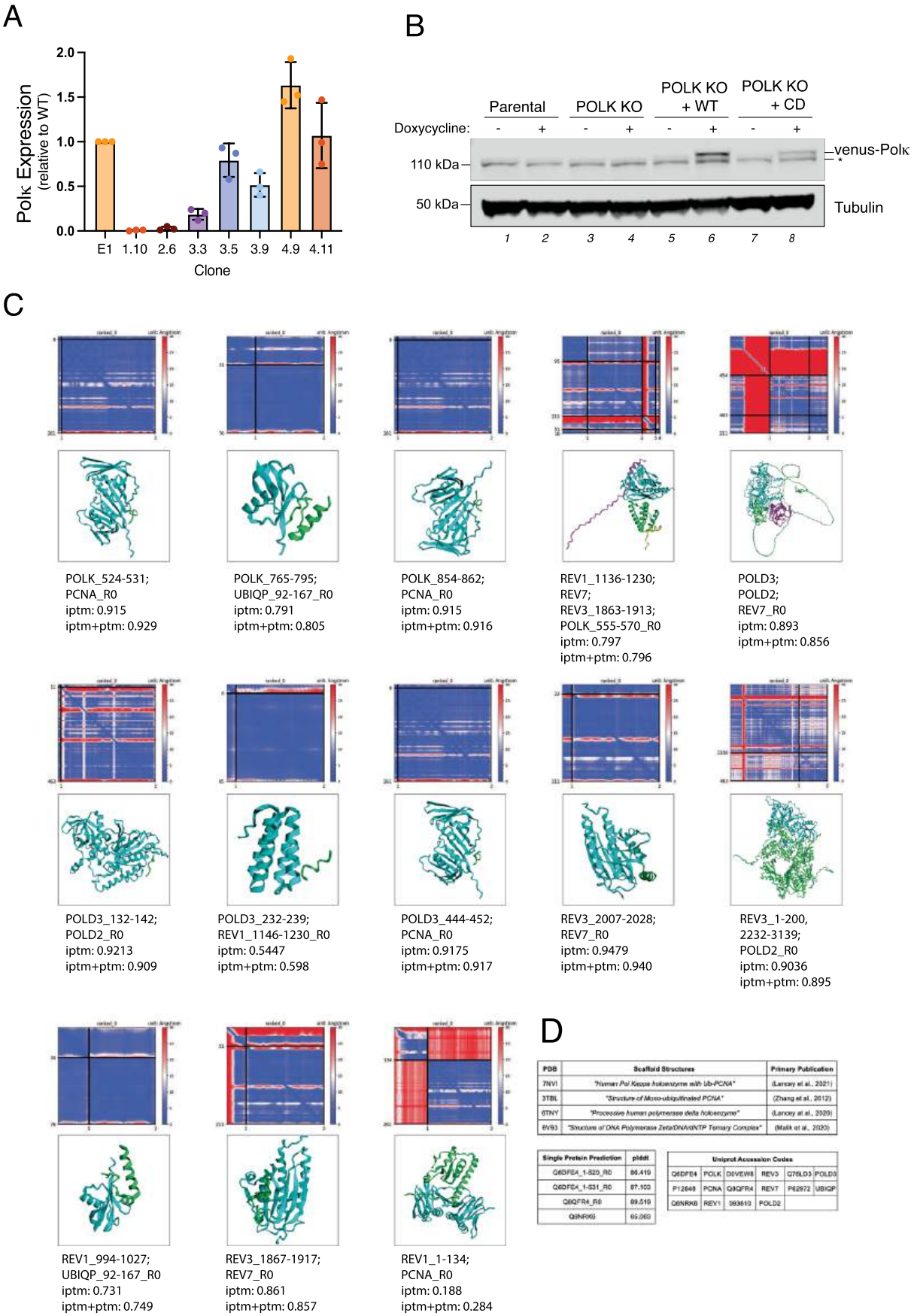

Extended Data Fig. 7 | See next page for caption.

https://doi.org/10.1038/s41594-024-01395-3

Extended Data Fig. 7 | a) Knockout of *POLK* in U2OS cells was validated by qPCR. Bar graphs represent *POLK* mRNA (cDNA) expression levels relative to WT parental cells (E1) and normalised to GAPDH expression levels. Error bars represent standard deviation from the mean of a technical triplicate PCR reaction (one representative experiment of two biological replicates is shown). Clones 1.10 was selected for further studies. **b**) Western blot analysis of whole cell extracts of the indicated cell lines treated with doxycycline where indicated. Note that we were unable to detect endogenous Polκ with three independent antibodies that were tested (A301-975A (Bethyl); A301-977A (Bethyl); sc-166667 (Santa Cruz). * indicates a non-specific band. **c)** AlphaPulldown predictions of protein complexes were utilised to construct the composite molecular models presented in Fig. 7. Each panel is divided into three sections: The upper panel displays the Predicted Aligned Error (PAE) plots associated with specific protein/fragment combinations generated by AlphaPulldown[77]. The PAE score in AlphaFold estimates the distance errors for residue pairs. It is represented by plots composed by diagonal squares for inner-correlation and cross-correlation areas for protein/fragment interactions. They assess prediction confidence, with low values being reliable and high values unreliable. The middle panel shows the predicted structures. Lastly, the lower panel includes the names of the predicted protein combinations, along with their corresponding Interface Predicted Template Modelling (IPTM), the Predicted Template Modelling (PTM) scores and the Ranking of the model (R0). **d)** Summary tables featuring the protein structures used as scaffolds for model building, along with their respective PDB codes. Single protein predictions obtained from AlphaPulldown with related Predicted Local Distance Difference Test scores (pLDDT). Uniprot accession codes for each of the proteins used for the complex protein modelling.

nature portfolio

Corresponding author(s): Julien P. Duxin NSMB-A48174

Last updated by author(s): 10/07/2024

Reporting Summary

Nature Portfolio wishes to improve the reproducibility of the work that we publish. This form provides structure for consistency and transparency in reporting. For further information on Nature Portfolio policies, see our Editorial Policies and the Editorial Policy Checklist.

Statistics

For all statistical analyses, confirm that the following items are present in the figure legend, table legend, main text, or Methods section.

n/a	Confirmed
☐	☒ The exact sample size (*n*) for each experimental group/condition, given as a discrete number and unit of measurement
☐	☒ A statement on whether measurements were taken from distinct samples or whether the same sample was measured repeatedly
☐	☒ The statistical test(s) used AND whether they are one- or two-sided *Only common tests should be described solely by name; describe more complex techniques in the Methods section.*
☒	☐ A description of all covariates tested
☐	☒ A description of any assumptions or corrections, such as tests of normality and adjustment for multiple comparisons
☐	☒ A full description of the statistical parameters including central tendency (e.g. means) or other basic estimates (e.g. regression coefficient) AND variation (e.g. standard deviation) or associated estimates of uncertainty (e.g. confidence intervals)
☐	☒ For null hypothesis testing, the test statistic (e.g. *F*, *t*, *r*) with confidence intervals, effect sizes, degrees of freedom and *P* value noted *Give P values as exact values whenever suitable.*
☒	☐ For Bayesian analysis, information on the choice of priors and Markov chain Monte Carlo settings
☒	☐ For hierarchical and complex designs, identification of the appropriate level for tests and full reporting of outcomes
☐	☒ Estimates of effect sizes (e.g. Cohen's *d*, Pearson's *r*), indicating how they were calculated

Our web collection on statistics for biologists contains articles on many of the points above.

Software and code

Policy information about availability of computer code

Data collection	No custom software was used. Western blots were acquired on an Amersham Imager 600 (GE Healthcare) with control software v1.2. Autoradiographs were visualized using a Typhoon FLA 7000 (GE healthcare) with control software v1.3. Mass spectrometry raw data were collected with Thermo Tune v1-1-117-26 and Thermo Xcalibur v4.3.73.11.
Data analysis	No custom software was used. All mass spectrometry raw data were analyzed using the freely available MaxQuant software (Cox and Mann, 2008), version 1.6.0.1, with the Xenopus laevis FASTA database downloaded from Uniprot on the 13th of May 2020 for the total proteome and UBIMAX experiments and on the 3rd of September 2021 for the IP-MS experiments. Quantification and statistical tests of the MaxQuant output files ("proteinGroups.txt") were performed using Perseus software (Tyanova et al., 2016), version 1.6.0.2, as was Pearson correlation, coefficients of variation, Principal Component, hierarchical clustering, and enrichment analyses. Protein networks were created using the online STRING database, version 11.5 (Szklarczyk et al., 2023). Autoradiographs were quantified using ImageJ, version 1.53t. Graphs and the statistical tests displayed in them were done in Prism (GraphPad), version 9.5.1.

For manuscripts utilizing custom algorithms or software that are central to the research but not yet described in published literature, software must be made available to editors and reviewers. We strongly encourage code deposition in a community repository (e.g. GitHub). See the Nature Portfolio guidelines for submitting code & software for further information.

Data

Policy information about availability of data

All manuscripts must include a data availability statement. This statement should provide the following information, where applicable:

- Accession codes, unique identifiers, or web links for publicly available datasets
- A description of any restrictions on data availability
- For clinical datasets or third party data, please ensure that the statement adheres to our policy

The mass spectrometry proteomics data have been deposited to the ProteomeXchange Consortium via the PRIDE partner repository (Perez-Riverol et al., 2022) with the following dataset identifier PXD044258.Source data are provided with this paper.

Research involving human participants, their data, or biological material

Policy information about studies with human participants or human data. See also policy information about sex, gender (identity/presentation), and sexual orientation and race, ethnicity and racism.

Reporting on sex and gender	*Use the terms sex (biological attribute) and gender (shaped by social and cultural circumstances) carefully in order to avoid confusing both terms. Indicate if findings apply to only one sex or gender; describe whether sex and gender were considered in study design; whether sex and/or gender was determined based on self-reporting or assigned and methods used. Provide in the source data disaggregated sex and gender data, where this information has been collected, and if consent has been obtained for sharing of individual-level data; provide overall numbers in this Reporting Summary. Please state if this information has not been collected. Report sex- and gender-based analyses where performed, justify reasons for lack of sex- and gender-based analysis.*
Reporting on race, ethnicity, or other socially relevant groupings	*Please specify the socially constructed or socially relevant categorization variable(s) used in your manuscript and explain why they were used. Please note that such variables should not be used as proxies for other socially constructed/relevant variables (for example, race or ethnicity should not be used as a proxy for socioeconomic status). Provide clear definitions of the relevant terms used, how they were provided (by the participants/respondents, the researchers, or third parties), and the method(s) used to classify people into the different categories (e.g. self-report, census or administrative data, social media data, etc.) Please provide details about how you controlled for confounding variables in your analyses.*
Population characteristics	*Describe the covariate-relevant population characteristics of the human research participants (e.g. age, genotypic information, past and current diagnosis and treatment categories). If you filled out the behavioural & social sciences study design questions and have nothing to add here, write "See above."*
Recruitment	*Describe how participants were recruited. Outline any potential self-selection bias or other biases that may be present and how these are likely to impact results.*
Ethics oversight	*Identify the organization(s) that approved the study protocol.*

Note that full information on the approval of the study protocol must also be provided in the manuscript.

Field-specific reporting

Please select the one below that is the best fit for your research. If you are not sure, read the appropriate sections before making your selection.

☒ Life sciences ☐ Behavioural & social sciences ☐ Ecological, evolutionary & environmental sciences

For a reference copy of the document with all sections, see nature.com/documents/nr-reporting-summary-flat.pdf

Life sciences study design

All studies must disclose on these points even when the disclosure is negative.

Sample size	Sample size calculation was not performed. Mass spectrometry experiments were performed in quadruplicate. The size of the individual samples (amount of protein starting material) was determined through pilot experiments. Biochemical analyses (western blots and autoradiographs) were performed at least in duplicate (independent egg extract reactions or independent cell cultures, as applicable).
Data exclusions	*Describe any data exclusions. If no data were excluded from the analyses, state so OR if data were excluded, describe the exclusions and the rationale behind them, indicating whether exclusion criteria were pre-established.*
Replication	Mass spectrometry experiments were performed in quadruplicate to ensure reproducibility, All western blot and autoradiographic analyses were performed at least in duplicate. All attempts at replication were successful. Colony assays were performed in triplicate.

Randomization	Samples were not divided into experimental groups. All replicates for all individual mass spectrometry experiments were simultaneously prepared, handled, and statistically processed while taking multiple-hypotheses testing into account. Further randomization was not considered relevant for the experimental design of the biochemical analyses of this study.
Blinding	All samples relating to each experiment were handled simultaneously. Samples were clearly labeled (and thus not blinded), which is important to both MS, western blot and autoradiographic experimental designs. During handling, all samples were numbered and processed in random order to avoid introduction of bias into the samples.

Reporting for specific materials, systems and methods

We require information from authors about some types of materials, experimental systems and methods used in many studies. Here, indicate whether each material, system or method listed is relevant to your study. If you are not sure if a list item applies to your research, read the appropriate section before selecting a response.

Materials & experimental systems

n/a	Involved in the study
☐	☒ Antibodies
☐	☒ Eukaryotic cell lines
☒	☐ Palaeontology and archaeology
☐	☒ Animals and other organisms
☒	☐ Clinical data
☒	☐ Dual use research of concern
☒	☐ Plants

Methods

n/a	Involved in the study
☒	☐ ChIP-seq
☒	☐ Flow cytometry
☒	☐ MRI-based neuroimaging

Antibodies

Antibodies used	See manuscript
Validation	See manuscript

Eukaryotic cell lines

Policy information about cell lines and Sex and Gender in Research

Cell line source(s)	U2OS Flp-In T-REx cells were kind gift from H. Piwnica-Worms
Authentication	The cell lines were not authenticated.
Mycoplasma contamination	The cell line used in this study was routinely tested negative for Mycoplasma contamination.
Commonly misidentified lines (See ICLAC register)	*Name any commonly misidentified cell lines used in the study and provide a rationale for their use.*

Animals and other research organisms

Policy information about studies involving animals; ARRIVE guidelines recommended for reporting animal research, and Sex and Gender in Research

Laboratory animals	Egg extracts were prepared using eggs (oocytes) collected from adult female Xenopus laevis frogs (Nasco Cat #LM0053MX).
Wild animals	This study did not involve wild animals.
Reporting on sex	Xenopus laevis frogs were solely used for the preparation of egg extract in this study. As only female frogs can produce and lay eggs, the use of male frogs were not considered for this study. Sex was assigned by the vendor (Nasco).
Field-collected samples	This study did not involve samples collected in the field.
Ethics oversight	All experiments involving animals were approved by the Danish Animal Experiments Inspectorate and are conform to relevant regulatory standards and European guidelines.

Note that full information on the approval of the study protocol must also be provided in the manuscript.

Plants

Seed stocks	*Report on the source of all seed stocks or other plant material used. If applicable, state the seed stock centre and catalogue number. If plant specimens were collected from the field, describe the collection location, date and sampling procedures.*
Novel plant genotypes	*Describe the methods by which all novel plant genotypes were produced. This includes those generated by transgenic approaches, gene editing, chemical/radiation-based mutagenesis and hybridization. For transgenic lines, describe the transformation method, the number of independent lines analyzed and the generation upon which experiments were performed. For gene-edited lines, describe the editor used, the endogenous sequence targeted for editing, the targeting guide RNA sequence (if applicable) and how the editor was applied.*
Authentication	*Describe any authentication procedures for each seed stock used or novel genotype generated. Describe any experiments used to assess the effect of a mutation and, where applicable, how potential secondary effects (e.g. second site T-DNA insertions, mosiacism, off-target gene editing) were examined.*